

Long Lived Light Scalars as Probe of Low Scale Seesaw Models

P. S. Bhupal Dev^a, Rabindra N. Mohapatra^b, Yongchao Zhang^c

^a *Department of Physics and McDonnell Center for the Space Sciences,
Washington University, St. Louis, MO 63130, USA*

^b *Maryland Center for Fundamental Physics, Department of Physics,
University of Maryland, College Park, MD 20742, USA*

^c *Service de Physique Théorique, Université Libre de Bruxelles,
Boulevard du Triomphe, CP225, 1050 Brussels, Belgium*

Abstract

We point out that in generic TeV scale seesaw models for neutrino masses with local $B - L$ symmetry breaking, there is a phenomenologically allowed range of parameters where the Higgs field responsible for $B - L$ symmetry breaking leaves a physical real scalar field with mass around GeV scale. This particle (denoted here by H_3) is weakly mixed with the Standard Model Higgs field (h) with mixing $\theta_1 \lesssim m_{H_3}/m_h$, barring fine-tuned cancellation. In the specific case when the $B - L$ symmetry is embedded into the TeV scale left-right seesaw scenario, we show that the bounds on the $h - H_3$ mixing θ_1 become further strengthened due to low energy flavor constraints, thus forcing the light H_3 to be long lived, with displaced vertex signals at the LHC. The property of left-right TeV scale seesaw models are such that they make the H_3 decay to two photons as the dominant mode. This is in contrast with a generic light scalar that mixes with the SM Higgs boson, which could also have leptonic and hadronic decay modes with comparable or larger strength. We discuss the production of this new scalar field at the LHC and show that it leads to testable displaced vertex signals of collimated photon jets, which is a new distinguishing feature of the left-right seesaw model. We also study a simpler version of the model where the $SU(2)_R$ breaking scale is much higher than the $\mathcal{O}(\text{TeV})$ $U(1)_{B-L}$ breaking scale, in which case the production and decay of H_3 proceed differently, but its long lifetime feature is still preserved for a large range of parameters. Thus, the search for such long-lived light scalar particles provides a new way to probe TeV scale seesaw models for neutrino masses at colliders.

Keywords: Neutrino Mass, Light Scalar, Displaced Vertex, Large Hadron Collider

Email addresses: bdev@wustl.edu (P. S. Bhupal Dev), rmohapat@umd.edu (Rabindra N. Mohapatra), yongchao.zhang@ulb.ac.be (Yongchao Zhang)

Preprint submitted to Nuclear Physics B

August 10, 2017

Contents

1	Introduction	3
2	Minimal left-right seesaw model	4
3	Light scalar in TeV-scale LR seesaw	5
3.1	Parameters for a light scalar	7
3.2	Radiative corrections	8
3.3	Couplings of H_3	9
3.4	Decay lifetime and branching ratios	11
4	Cosmological constraints	14
5	Laboratory constraints	15
5.1	K and B meson oscillations	15
5.2	Meson decay	17
5.2.1	K meson decay	20
5.2.2	B meson decay	21
5.2.3	Beam-dump experiments	25
5.3	SM Higgs, Z and top decays	26
6	Production and displaced vertex searches at colliders	28
6.1	Production cross section	28
6.2	Prospects at the LHC	29
6.3	Prospects at future 100 TeV collider	31
6.4	Probing the LR seesaw model	32
7	Light neutral scalar in $U(1)_{B-L}$ model	34
7.1	Couplings and decay	35
7.2	Meson limits	36
7.3	Production and LLP searches	36
8	Conclusion	40
Appendix A	Partial decay widths of H_3	42
Appendix B	Rare Z decay $Z \rightarrow \gamma H_3$	43
Appendix C	Light RH neutrinos in the LR seesaw model	44

1. Introduction

Seesaw mechanism seems to provide a very simple and elegant way to understand the smallness of neutrino masses [1–5]. Two key ingredients of this mechanism are: (i) addition of the right-handed neutrinos (RHN) to the Standard Model (SM), and (ii) a large Majorana mass for the RHNs which breaks the accidental $B - L$ symmetry of the SM. There exist a large class of well-motivated ultraviolet (UV)-complete seesaw models which necessarily employ local $B - L$ symmetry, e.g. the TeV-scale left-right (LR) symmetric model [6–8]. It will therefore be an important step to find experimental evidence for the $B - L$ symmetry and its breaking. If the local $B - L$ is broken by a Higgs field that carries this quantum number, there will be a remnant neutral scalar field, denoted here by H_3 (for reasons explained below), analogous to the Higgs boson h of the SM. So looking for signatures of H_3 can provide invaluable clues to the nature of the new physics associated with neutrino mass generation. Clearly, such a search is realistic only if the $B - L$ symmetry breaking scale is within the multi-TeV range.

The mass and couplings of the new Higgs field are still unrestricted to a large extent, mainly because it communicates to the SM sector only through its mixing with the SM Higgs and via the heavy gauge boson interactions. The mass range heavier than the SM Higgs boson has been discussed earlier [9–12]. The mass range near m_h would generically lead to large $h - H_3$ mixing, which is disfavored by the LHC Higgs data [13]. So we will focus here on the more interesting regime with $m_{H_3} \ll m_h$ in which case, the $H_3 - h$ mixing angle $\theta_1 \lesssim m_{H_3}/m_h \simeq 8 \times 10^{-3}(m_{H_3}/\text{GeV})$ from considerations of fine tuning. Smaller values of θ_1 can be analyzed as part of the allowed parameter range of generic $B - L$ models. However, as we show here, this range is naturally dictated to us from low energy flavor constraints, once the $B - L$ symmetry is embedded into the minimal LR model. This leads to the H_3 particle being necessarily long-lived, with interesting displaced vertex signals at the Large Hadron Collider (LHC). The important point is that even though a generic light scalar in a BSM theory that mixes with the SM Higgs can have leptonic, hadronic as well as photonic decay modes, the specific property of LR seesaw models makes the two photon decay mode exclusively dominant, as recently pointed out by us [14]. In this paper, we elaborate on the details of this scenario, including an in-depth discussion of all relevant high and low-energy constraints on the model parameter space, the production and decay of the new Higgs boson at the LHC and future colliders, as well as the experimental prospects for observing the displaced vertex collimated diphoton signal. We would like to emphasize the complementarity of the new collider signal discussed here with existing and future low-energy probes of light neutral sectors at the intensity frontier.

We will discuss two classes of UV-complete theories, based on (i) the full LR gauge group $SU(2)_L \times SU(2)_R \times U(1)_{B-L}$, and (ii) a simpler $B - L$ model with $SU(2)_L \times U(1)_{I_{3R}} \times U(1)_{B-L}$ local symmetry. The bulk of this paper deals with the class (i), where we consider a LR symmetric model where parity is broken at a much higher scale than the $SU(2)_R$ breaking. As a result, the $SU(2)_L$ Higgs triplet of the familiar left-right model is pushed to a much higher scale and also in neutrino mass formula, type I seesaw dominates. The heavy-light neutrino mixing is a separate parameter in the model and is small i.e. $\sim \sqrt{m_\nu/m_N} \lesssim 10^{-5.5}$

in the kinematic region where m_{H_3} is less than 10 GeV and much less than the RH neutrino masses (assumed to be of order of 1 TeV), so its contribution to the H_3 phenomenology can be ignored.

The class (ii) scenario that we discuss can be thought of as an “effective” theory of the LR model, where the $SU(2)_R$ symmetry breaking scale is much higher than the $U(1)_{B-L}$ -breaking which is assumed to be at the TeV-scale to be accessible experimentally. Nevertheless, our results for the $U(1)_{B-L}$ case are applicable to a wider class of Z' -models, which have an associated Higgs boson that mixes with SM Higgs field.

The rest of the paper is organized as follows: in Section 2, we briefly review the minimal LR seesaw model and set up our notation. In Section 3, we present the arguments for the light $B-L$ breaking Higgs being weakly mixed with the SM Higgs h and the heavy CP-even Higgs H_1 , and study its decay lifetime and branching ratios. In Section 4, we derive a lower limit on the light scalar H_3 mass from cosmological considerations at the nucleosynthesis epoch. In Section 5, we present an in-depth analysis of all available laboratory constraints on the light scalar parameter space. In Section 6, we discuss the production of H_3 at hadron colliders and its detection prospects at the LHC, as well as in future colliders. In Section 7, we analyze the LLP prospects of a simpler $U(1)_{B-L}$ model. Our conclusions are given in Section 8. In Appendix A, we collect the two-body partial decay widths of H_3 in the LR model, and in Appendix B, the partial decay width of the loop-induced process $Z \rightarrow H_3\gamma$. Finally, in Appendix C, we study the LLP sensitivity of light RHNs in the LR model at the LHC.

2. Minimal left-right seesaw model

For completeness and to set up our notation, we briefly review the minimal LR model [6–8] in this section, based on the gauge group $SU(3)_c \times SU(2)_L \times SU(2)_R \times U(1)_{B-L}$ with parity broken at a higher scale than $SU(2)_R$. The quarks and leptons are assigned to the following irreducible representations:

$$Q_{L,i} = \begin{pmatrix} u_L \\ d_L \end{pmatrix}_i : \left(\mathbf{3}, \mathbf{2}, \mathbf{1}, \frac{1}{3} \right), \quad Q_{R,i} = \begin{pmatrix} u_R \\ d_R \end{pmatrix}_i : \left(\mathbf{3}, \mathbf{1}, \mathbf{2}, \frac{1}{3} \right), \quad (1)$$

$$\psi_{L,i} = \begin{pmatrix} \nu_L \\ e_L \end{pmatrix}_i : \left(\mathbf{1}, \mathbf{2}, \mathbf{1}, -1 \right), \quad \psi_{R,i} = \begin{pmatrix} N_R \\ e_R \end{pmatrix}_i : \left(\mathbf{1}, \mathbf{1}, \mathbf{2}, -1 \right), \quad (2)$$

where $i = 1, 2, 3$ represents the family index, and the subscripts L, R denote the left- and right-handed chiral projection operators $P_{L,R} = (1 \mp \gamma_5)/2$, respectively. There are different ways to break the $SU(2)_R \times U(1)_{B-L}$ gauge symmetry and to understand the small neutrino masses in this model, depending on the choice of the Higgs fields. One of the simplest choices is to introduce $SU(2)_L \times SU(2)_R$ bi-doublet and $SU(2)_R$ triplet scalars

$$\Phi = \begin{pmatrix} \phi_1^0 & \phi_2^+ \\ \phi_1^- & \phi_2^0 \end{pmatrix} : \left(\mathbf{1}, \mathbf{2}, \mathbf{2}, 0 \right), \quad \Delta_R = \begin{pmatrix} \Delta_R^+/\sqrt{2} & \Delta_R^{++} \\ \Delta_R^0 & -\Delta_R^+/\sqrt{2} \end{pmatrix} : \left(\mathbf{1}, \mathbf{1}, \mathbf{3}, 2 \right), \quad (3)$$

respectively, with the neutral components of the above fields acquiring non-zero vacuum expectation values (VEV):

$$\langle \Delta_R^0 \rangle = v_R, \quad \langle \phi_1^0 \rangle = \kappa, \quad \langle \phi_2^0 \rangle = \kappa', \quad (4)$$

with the electroweak (EW) VEV given by $v_{\text{EW}} = \sqrt{\kappa^2 + \kappa'^2} \simeq 174$ GeV. We assume the v_R scale to be in the multi-TeV range for phenomenological purposes. This is the version of the LR seesaw that results when parity symmetry is broken at a much higher scale than $SU(2)_R$ [15] which, as remarked earlier, removes the $\Delta_L(\mathbf{1}, \mathbf{3}, \mathbf{1}, 2)$ Higgs field from the effective low energy theory. This makes it simpler to analyze and present our main results, although our conclusions remain unchanged in the fully parity symmetric version being a TeV scale theory.

The fermion masses can be understood from the Yukawa Lagrangian:

$$\begin{aligned} \mathcal{L}_Y = & h_{q,ij} \bar{Q}_{L,i} \Phi Q_{R,j} + \tilde{h}_{q,ij} \bar{Q}_{L,i} \tilde{\Phi} Q_{R,j} + h_{\ell,ij} \bar{\psi}_{L,i} \Phi \psi_{R,j} + \tilde{h}_{\ell,ij} \bar{\psi}_{L,i} \tilde{\Phi} \psi_{R,j} \\ & + f_{ij} \psi_{R,i}^T C i \sigma_2 \Delta_R \psi_{R,j} + \text{H.c.}, \end{aligned} \quad (5)$$

where $\tilde{\Phi} = i\sigma_2 \Phi^*$ (with σ_2 being the second Pauli matrix) and C stands for charge conjugation. The standard type-I seesaw mass matrix for neutrinos follows from the leptonic part of the above couplings after symmetry breaking. The triplet VEV v_R breaks lepton number and provides the Majorana mass for the heavy RHNs which goes into the seesaw matrix [2].

3. Light scalar in TeV-scale LR seesaw

In this section, we analyze the TeV-scale LR seesaw parameter space for a light scalar with mass in the (sub) GeV range and its couplings to determine the decay branching ratios and lifetime.

The most general scalar potential for this model reads as follows:

$$\begin{aligned} \mathcal{V} = & -\mu_1^2 \text{Tr}(\Phi^\dagger \Phi) - \mu_2^2 \left[\text{Tr}(\tilde{\Phi} \Phi^\dagger) + \text{Tr}(\tilde{\Phi}^\dagger \Phi) \right] - \mu_3^2 \text{Tr}(\Delta_R \Delta_R^\dagger) \\ & + \lambda_1 \left[\text{Tr}(\Phi^\dagger \Phi) \right]^2 + \lambda_2 \left\{ \left[\text{Tr}(\tilde{\Phi} \Phi^\dagger) \right]^2 + \left[\text{Tr}(\tilde{\Phi}^\dagger \Phi) \right]^2 \right\} \\ & + \lambda_3 \text{Tr}(\tilde{\Phi} \Phi^\dagger) \text{Tr}(\tilde{\Phi}^\dagger \Phi) + \lambda_4 \text{Tr}(\Phi^\dagger \Phi) \left[\text{Tr}(\tilde{\Phi} \Phi^\dagger) + \text{Tr}(\tilde{\Phi}^\dagger \Phi) \right] \\ & + \rho_1 \left[\text{Tr}(\Delta_R \Delta_R^\dagger) \right]^2 + \rho_2 \text{Tr}(\Delta_R \Delta_R) \text{Tr}(\Delta_R^\dagger \Delta_R^\dagger) \\ & + \alpha_1 \text{Tr}(\Phi^\dagger \Phi) \text{Tr}(\Delta_R \Delta_R^\dagger) + \left[\alpha_2 e^{i\delta_2} \text{Tr}(\tilde{\Phi} \Phi^\dagger) \text{Tr}(\Delta_R \Delta_R^\dagger) + \text{H.c.} \right] + \alpha_3 \text{Tr}(\Phi^\dagger \Phi \Delta_R \Delta_R^\dagger). \end{aligned} \quad (6)$$

All the 12 parameters $\mu_{1,2,3}^2$, $\lambda_{1,2,3,4}$, $\rho_{1,2}$, $\alpha_{1,2,3}$ are chosen to be real, with an appropriate redefinition of the fields, and the only CP-violating phase δ_2 is associated with the coupling α_2 , as explicitly shown in Eq. (6). There are 14 scalar degrees of freedom, six of which are Goldstone modes eaten by the W^\pm , W_R^\pm , Z , Z_R gauge bosons, thus leaving 8 physical Higgs bosons, denoted by $h, H_1, A_1, H_3, H_1^\pm$ and $H_2^{\pm\pm}$. The full scalar potential for this class of

LR seesaw models was analyzed in detail in Refs. [10, 11, 16] and here we present only the results relevant for our purpose.

We work in the natural parameter space, where the following parameters are small:

$$\xi \equiv \kappa'/\kappa = \frac{m_b}{m_t} \ll 1, \quad \epsilon \equiv \kappa'/v_R \ll v_{\text{EW}}/v_R \ll 1, \quad (7)$$

and also assume that there is no CP-violation in the scalar sector, i.e. the CP-violating phase δ_2 is zero. There are 6 degrees of freedom in the neutral scalar sector: three dominantly CP-even and the other three CP-odd. This includes the two Goldstone modes eaten by the neutral Z and Z_R gauge bosons. In the CP-even sector of neutral scalars, after applying the minimization conditions with respect to the three VEVs κ , κ' , v_R and the phase δ_2 associated with the VEV κ' , we obtain the squared mass matrices in the basis of $\{\phi_1^{0\text{Re}}, \phi_2^{0\text{Re}}, \Delta_R^{0\text{Re}}\}$ at the zeroth, first and second order of the small parameters ξ and ϵ defined in Eq. (7) (setting the phase δ_2 to be zero), respectively,

$$(\mathcal{M}_0^2)^{(0)} = v_R^2 \begin{pmatrix} 0 & 0 & 0 \\ 0 & \alpha_3 & 0 \\ 0 & 0 & 4\rho_1 \end{pmatrix}, \quad (8)$$

$$(\mathcal{M}_0^2)^{(1)} = v_R^2 \begin{pmatrix} 0 & -\alpha_3\xi & 2\alpha_1\epsilon \\ -\alpha_3\xi & 0 & 4\alpha_2\epsilon \\ 2\alpha_1\epsilon & 4\alpha_2\epsilon & 0 \end{pmatrix}, \quad (9)$$

$$(\mathcal{M}_0^2)^{(2)} = v_R^2 \begin{pmatrix} 4\lambda_1\epsilon^2 + \alpha_3\xi^2 & 4\lambda_4\epsilon^2 & 4\alpha_2\epsilon\xi \\ 4\lambda_4\epsilon^2 & 4(2\lambda_2 + \lambda_3)\epsilon^2 + \alpha_3\xi^2 & 2(\alpha_1 + \alpha_3)\epsilon\xi \\ 4\alpha_2\epsilon\xi & 2(\alpha_1 + \alpha_3)\epsilon\xi & 0 \end{pmatrix}. \quad (10)$$

In the limit of $\xi \ll 1$, one of the scalars, predominantly from $\phi_2^{0\text{Re}}$ is heavy, with mass at the v_R scale $\sqrt{\alpha_3}v_R$ and decouples from the lower energy SM sector, thus leading to a reduced scalar mass matrix involving only $\phi_1^{0\text{Re}}$ and $\Delta_R^{0\text{Re}}$. If the quartic coupling ρ_1 is large, say of order one, then $\Delta_R^{0\text{Re}}$ (denoted here by H_3) will also be heavy, close to the v_R scale, and its mixing with the SM Higgs boson h will be given by $\theta_1 \simeq \frac{\alpha_1 v_{\text{EW}}}{\rho_1 v_R}$. However, there exists another possibility, mainly motivated by the lack of any direct experimental constraints on its mass, as well as supported by arguments based on radiative stability (see Section 3.2), where H_3 could also be very light, and in particular, lighter than the SM Higgs boson. This happens when $\rho_1 \ll 1$, in which case, the sub-matrix in the basis of $\{\phi_1^{0\text{Re}}, \Delta_R^{0\text{Re}}\}$ becomes

$$\mathcal{M}_0^2 \simeq \begin{pmatrix} 4\lambda_1\epsilon^2 & 2\alpha_1\epsilon \\ 2\alpha_1\epsilon & 4\rho_1 \end{pmatrix} v_R^2. \quad (11)$$

In the limit of $m_{H_3}^2 \ll m_h^2$, Eq. (11) can be diagonalized in a seesaw-like approximation, and the two scalar masses are respectively given by

$$m_h^2 \simeq 4\lambda_1\epsilon^2 v_R^2 = 4\lambda_1 v_{\text{EW}}^2, \quad (12)$$

$$m_{H_3}^2 \simeq 4\rho_1 v_R^2 - \sin^2 \theta_1 m_h^2, \quad (13)$$

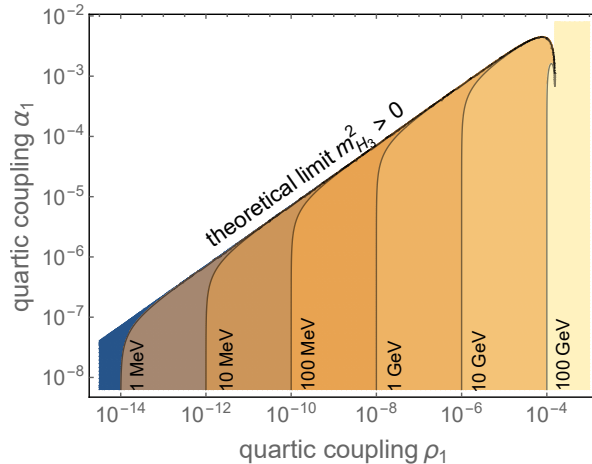


Figure 1: Contours of m_{H_3} as a function of the quartic coupling parameters ρ_1 and α_1 defined in the scalar potential (6). Here we have set the RH triplet VEV $v_R = 5$ TeV.

with the mixing angle

$$\sin \theta_1 \simeq \frac{\alpha_1}{2\lambda_1 \epsilon} = \frac{\alpha_1}{2\lambda_1} \frac{v_R}{v_{EW}}. \quad (14)$$

Note that the mixing has an inverted dependence on the VEV ratio $(v_{EW}/v_R)^{-1}$, compared to the case where $m_{H_3} \gg m_h$. This restricts the parameter α_1 to be appropriately small in order to ensure that $\sin \theta_1 \leq 1$, as we show below.

3.1. Parameters for a light scalar

The question that we address in this subsection is whether there is a range of parameters in the model where H_3 could be light, i.e. in the (sub)-GeV range, which has important phenomenological ramifications. From Eq. (13), it is clear that the lightness of H_3 depends on how small the values of ρ_1 and α_1 can be:

$$m_{H_3}^2 \simeq \left(4\rho_1 - \frac{\alpha_1^2}{\lambda_1} \right) v_R^2. \quad (15)$$

The exact dependence of m_{H_3} on the parameters ρ_1 and α_1 is shown in Figure 1 for a representative value of $v_R = 5$ TeV, which is close to the smallest possible value allowed by the current direct [17–19] and indirect [20] constraints on the W_R mass (with appropriate scaling for $g_R \neq g_L$, where $g_{L,R}$ are the $SU(2)_{L,R}$ gauge couplings). We see that for $\rho_1 \sim 10^{-8}$ and $\alpha_1 \lesssim 10^{-5}$, we get $m_{H_3} \sim \mathcal{O}(\text{GeV})$, which is the region of great interest for long-lived particle (LLP) searches, as we will see below. For a small mixing $\sin \theta_1$, the H_3 mass is determined completely by ρ_1 which is required to be very small for light H_3 . However, when the mixing is sizable, i.e. α_1 is comparatively large, there can be large cancellation between the two terms in Eq. (13).

3.2. Radiative corrections

In this subsection, we consider the one-loop corrections to the H_3 mass to see whether $m_{H_3} \sim \mathcal{O}(\text{GeV})$ is radiatively stable. The one-loop renormalization group (RG) running of the gauge, quartic and Yukawa couplings in the LR model has been considered in Refs. [21–23]. Due to the large number of parameters in the scalar potential, some of the couplings would easily become non-perturbative before reaching up to the GUT or Planck scale, especially when the RH scale v_R is relatively low [16]. There are also stability and perturbativity constraints on some of the quartic couplings [24], but the mass of H_3 , which is proportional to $\sqrt{\rho_1}$ at the leading order at tree level [cf. Eq. (15)], is not limited by these arguments. Moreover, even if the gauge symmetry $SU(2)_R$ is restored at the few-TeV scale, the LR model is far from being a UV-complete theory up to the GUT scale, and more fields have to be introduced at higher energy scales, which hardly leave any imprints at the TeV scale. Our aim here is not to analyze the ultimate UV-complete theory with parity, rather we remain at the TeV-scale, and using the Coleman-Weinberg effective potential approach [25], check how the mass of H_3 would be affected by interacting with other particles in the TeV-scale LR model at the one-loop level.

Our considerations are similar to what happens to the SM Higgs mass. It is well known that if we neglect the one-loop fermion contributions to the Coleman-Weinberg effective potential, there would be a lower limit of order of 5 GeV on the Higgs boson mass [26, 27]. However, this bound goes away once the large top-quark Yukawa coupling is included. This approach for the LR models for the case of doublet Higgs but without singlet fermions was carried out in Ref. [28], where a lower bound on the heavy neutral Higgs of the order of 900 GeV was obtained. The crucial difference in our model is the fermion contribution, which enables us to avoid this lower bound on m_{H_3} .

In the Coleman-Weinberg effective potential, we find that the dominant one-loop corrections to $m_{H_3}^2$ arise from its gauge interaction with the heavy W_R, Z_R RH gauge bosons, the Yukawa interaction with the RHNs, and the interactions with the heavy scalars H_1, A_1, H_1^\pm and $H_2^{\pm\pm}$. All the interactions with the SM fields are suppressed by the small mixing angles. The Feynman diagrams of loop corrections to $m_{H_3}^2$ from the heavy particle loops are collected in Figure 2, which sum up to

$$(m_{H_3}^2)^{\text{loop}} \simeq \frac{3}{2\pi^2} \left[\frac{1}{3}\alpha_3^2 + \frac{8}{3}\rho_2^2 - 8f^4 + \frac{1}{2}g_R^4 + (g_R^2 + g_{BL}^2)^2 \right] v_R^2, \quad (16)$$

where g_{BL} is the $SU(2)_R$ and $U(1)_{B-L}$ gauge coupling strength, f is the RHN Yukawa coupling as defined in Eq. (5), and α_3 and ρ_2 are the scalar quartic couplings defined in Eq. (6). Without any tuning of the scalar, gauge and Yukawa couplings, the loop correction to m_{H_3} is expected to be of order $v_R/4\pi$. In the above expression, we have kept only the contribution of the scalar coupling α_3 since that is the only coupling which is expected to be of order one to satisfy the flavor changing neutral current (FCNC) constraints on bidoublet Higgs mass, as we will discuss below in Section 5. The important point here is that with the minus sign for the f contribution in Eq. (16), the bosonic and fermionic contributions can be made to cancel each other keeping H_3 mass light even in the presence of radiative

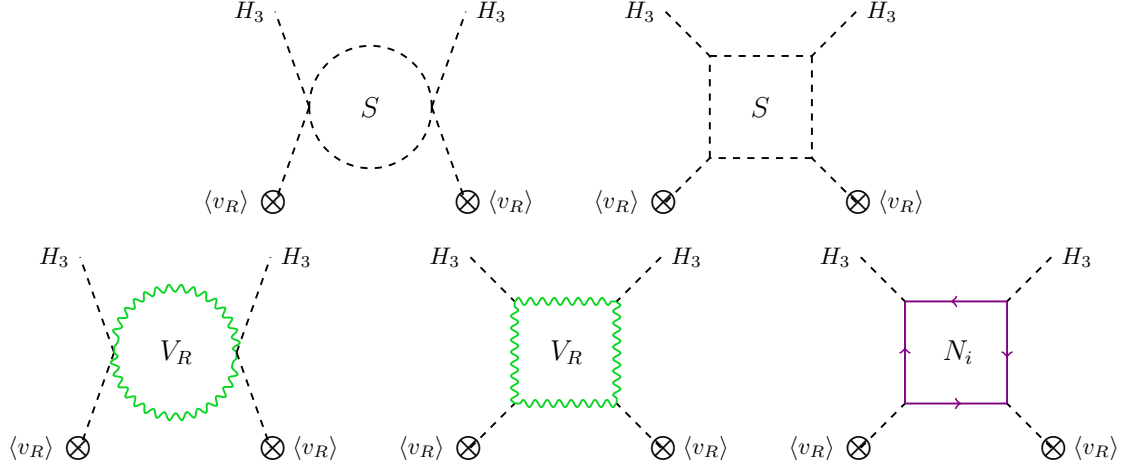


Figure 2: Dominant loop corrections to $m_{H_3}^2$ from interacting with the heavy scalars S ($H_1, A_1, H_1^\pm, H_2^{\pm\pm}$), the heavy gauge bosons V_R (W_R, Z_R) and the heavy RHNs N_i .

corrections. With a tuning of order $\text{GeV}/\frac{v_R}{4\pi} \sim 10^{-2}$ (with v_R at the TeV-scale) for the parameters in Eq. (16), we could easily obtain a light scalar H_3 at or below the GeV scale.

3.3. Couplings of H_3

In order to study the collider phenomenology of light H_3 , it is essential to delineate its couplings to various particles in the theory. In the limit of zero CP phase δ_2 in Eq. (6), H_3 could only mix with the scalars h and H_1 :

$$\begin{pmatrix} h \\ H_1 \\ H_3 \end{pmatrix} = \begin{pmatrix} 1 - \frac{1}{2}\xi^2 & \xi & -\sin\theta_1 \\ -\xi & 1 - \frac{1}{2}\xi^2 & -\sin\theta_2 \\ \sin\theta_1 & \sin\theta_2 & 1 \end{pmatrix} \begin{pmatrix} \phi_1^{0\text{Re}} \\ \phi_2^{0\text{Re}} \\ \Delta_R^{0\text{Re}} \end{pmatrix}, \quad (17)$$

where $\sin\theta_1$ is the $h - H_3$ mixing already defined in Eq. (14) and

$$\sin\theta_2 \simeq \frac{4\alpha_2\epsilon}{\alpha_3} = \frac{4\alpha_2}{\alpha_3} \frac{v_{\text{EW}}}{v_R}. \quad (18)$$

is the mixing between H_3 and H_1 . Both θ_1 and θ_2 are expected to be small for a GeV-scale H_3 . The ‘‘effective’’ mixing angles of H_3 responsible for the flavor conserving and violating couplings to the SM quarks and charged leptons can be defined as

$$\sin\tilde{\theta}_1 \equiv \sin\theta_1 + \xi \sin\theta_2, \quad (19)$$

$$\sin\tilde{\theta}_2 \equiv \sin\theta_2 + \xi \sin\theta_1, \quad (20)$$

which will be used in our subsequent discussion.

For completeness we collect all the coupling of light H_3 in the minimal LR models in Table 1, which is based on the calculation of Ref. [11] and up to the leading order in the

Table 1: The couplings of the light scalar H_3 , up to the leading order in ϵ and ξ .

couplings	values
$H_3 h h$	$\frac{1}{\sqrt{2}} \alpha_1 v_R$
$h H_3 H_3$	$-\sqrt{2} \alpha_1 v_{EW}$
$H_3 h H_1^0$	$2\sqrt{2} \alpha_2 v_R$
$H_3 H_1^0 H_1^0$	$\frac{1}{\sqrt{2}} \alpha_3 v_R$
$H_3 A_1^0 A_1^0$	$\frac{1}{\sqrt{2}} \alpha_3 v_R$
$H_3 H_1^+ H_1^-$	$\sqrt{2} \alpha_3 v_R$
$H_3 H_2^{++} H_2^{--}$	$2\sqrt{2} (\rho_1 + 2\rho_2) v_R$
$H_3 \bar{u} u$	$\frac{1}{\sqrt{2}} \widehat{Y}_U \sin \tilde{\theta}_1 - \frac{1}{\sqrt{2}} \left(V_L \widehat{Y}_D V_R^\dagger \right) \sin \tilde{\theta}_2$
$H_3 \bar{d} d$	$\frac{1}{\sqrt{2}} \widehat{Y}_D \sin \tilde{\theta}_1 - \frac{1}{\sqrt{2}} \left(V_L^\dagger \widehat{Y}_U V_R \right) \sin \tilde{\theta}_2$
$H_3 \bar{e} e$	$\frac{1}{\sqrt{2}} \widehat{Y}_E \sin \tilde{\theta}_1 - \frac{1}{\sqrt{2}} Y_{\nu N} \sin \tilde{\theta}_2$
$H_3 N N$	$\frac{m_N}{\sqrt{2} v_R}$
$H_3 W^+ W^-$	$\frac{1}{\sqrt{2}} g_L^2 \sin \theta_1 v_{EW} + \sqrt{2} g_R^2 \sin^2 \zeta_W v_R$
$H_3 W^+ W_R^-$	$\sqrt{2} g_R^2 \sin \zeta_W v_R$
$H_3 W_R^+ W_R^-$	$\sqrt{2} g_R^2 v_R$
$H_3 Z Z$	$\frac{g_L^2 \sin \theta_1 v_{EW}}{2\sqrt{2} \cos^2 \theta_w} + \frac{\sqrt{2} g_R^2 \sin^2 \zeta_Z v_R}{\cos^2 \phi}$
$H_3 Z Z_R$	$-\frac{g_L g_R \sin \theta_1 \cos \phi v_{EW}}{\sqrt{2} \cos \theta_w} + \frac{2\sqrt{2} g_R^2 \sin \zeta_Z v_R}{\cos^2 \phi}$
$H_3 Z_R Z_R$	$\frac{\sqrt{2} g_R^2 v_R}{\cos^2 \phi}$
$H_3 H_1^+ W^-$	$\frac{1}{2} g_L (\sin \theta_2 - \sin \theta_1 \xi)$
$H_3 H_1^+ W_R^-$	$\frac{1}{2} g_R \epsilon$
$H_3 A_1 Z$	$-\frac{i g_L (\sin \theta_2 - \sin \theta_1 \xi)}{2 \cos \theta_w}$
$H_3 A_1 Z_R$	$\frac{i}{2} g_R (\sin \theta_2 - \sin \theta_1 \xi) \cos \phi$

small parameters ξ and ϵ defined in Eq. (7). Here the RH gauge mixing ϕ is defined as $\tan \phi \equiv g_{BL}/g_R$, and the $W - W_R$ and $Z - Z_R$ mixings are respectively given by

$$\tan \zeta_W \simeq -\frac{2g_R \xi}{g_L} \left(\frac{m_W}{m_{W_R}} \right)^2, \quad (21)$$

$$\tan \zeta_Z \simeq \left[\frac{g_R^2}{g_L^2} - \left(1 + \frac{g_R^2}{g_L^2} \right) \sin^2 \theta_w \right]^{1/2} \left(\frac{m_Z}{m_{Z_R}} \right)^2, \quad (22)$$

where θ_w is the weak mixing angle.

In Table 1, the couplings to the charged leptons depend on the neutrino sector via the Dirac coupling matrix $Y_{\nu N} = m_D/v_{EW}$, which can be parameterized through the Casas-Ibarra form [29]

$$m_D = i m_N^{1/2} O m_\nu^{1/2} \quad (23)$$

with O an arbitrary complex orthogonal matrix, m_ν and m_N are the light neutrino and RHN mass matrix, respectively. Without fine-tuning, the Dirac Yukawa couplings $Y_{\nu N}$, and hence, the light-heavy neutrino mixing, are expected to be small for TeV-scale RH neutrinos. So we can safely ignore those couplings involving higher powers of $Y_{\nu N}$, such as $H_3\nu\nu$.

3.4. Decay lifetime and branching ratios

Through the mixing with the SM Higgs and the heavy scalar H_1 via respectively the mixing angles $\sin\theta_1$ and $\sin\theta_2$ in Eq. (14) and (18), a light H_3 could decay at tree level into the SM fermions,¹ through the Yukawa couplings in Table 1. Note that the couplings to quarks could be flavor-changing, depending on the magnitude of effective mixing angle $\sin\tilde{\theta}_2$, while the lepton flavor violating (LFV) couplings are proportional to the Dirac coupling $Y_{\nu N}$ and $\sin\tilde{\theta}_2$. At the one-loop level, the Yukawa couplings to the SM fermions induce the decay into digluon and diphoton, i.e. $H_3 \rightarrow gg, \gamma\gamma$, analogous to the SM Higgs. Considering the flavor limits on the mixing angles $\sin\theta_{1,2}$ below in Section 5, the fermion loops for both the $\gamma\gamma$ and gg channels are highly suppressed. However, for the decay $H_3 \rightarrow \gamma\gamma$, there are extra contributions from the heavy W_R^\pm, H_1^\pm and $H_2^{\pm\pm}$ loops. In the low mass limit $m_{H_3} \ll v_R$, the diphoton channel is sensitive only to the RH scale $\Gamma_{\gamma\gamma} \propto v_R^{-2}$ [32] and dominated by the W_R loop for TeV range v_R , as the scalar loops are comparatively suppressed by the loop function $5A_0(0)/A_1(0) = -5/21$ [cf. Eq. (A.3)]. Similarly, the SM W loop is highly suppressed by the small $W - W_R$ mixing $\sin\zeta_W$ [cf. Eq. (21)]. The dominant two-body tree- and loop-level decay channels of H_3 covering all the parameter space of interest for a light scalar $m_{H_3} \lesssim m_h$ are presented in Appendix A, while the other decay channels, such as $H_3 \rightarrow h^*h^* \rightarrow bbbb$, are suppressed either kinematically or by the multi-particle phase space.

The decay branching ratios (BR) of H_3 to the $qq, \ell^+\ell^-, \gamma\gamma$ and gg channels are presented in Figure 3 as functions of its mass and mixing with h (top panel) and H_1 (bottom panel). For concreteness, we have made the following reasonable assumptions: (i) The RH scale $v_R = 5$ TeV, which is close to the smallest value allowed by the current constraints on W_R . (ii) In the minimal LR model, the RH quark mixing matrix V_R is very similar to the CKM matrix V_L , up to some additional phases [33, 34]. For simplicity, we adopt $V_R = V_L$ in the calculation. Thus with the experimental values of the SM quark masses and CKM mixing, we obtain the numerical values of the H_3 couplings to the SM quarks, including the FCNC couplings, arising from its mixing with the heavy scalar H_1 [cf. Table 1]. (iii) The couplings of H_3 to the charged leptons depend on the heavy and light neutrino masses and their mixings via the Yukawa coupling matrix $Y_{\nu N}$. Here we assume the three light neutrino masses are of normal hierarchy with the lightest one to be 0.01 eV, while all the three RHNs are assumed to be degenerate at 1 TeV without any RH lepton mixing, which

¹ We assume here that all the three RHNs (typically at the TeV scale) are heavier than the light scalar H_3 , and therefore, the H_3 decay into RHNs is kinematically forbidden. Allowing for the $H_3 \rightarrow NN$ decay could lead to additional lepton number violating signatures, as discussed in Refs. [30, 31]. In addition, H_3 could in principle decays into the light neutrinos (or one light neutrino plus one heavy neutrino) through the heavy-light neutrino mixing $V_{\nu N} \simeq m_D M_N^{-1}$. However, for the TeV-scale type-I seesaw without any fine-tuning in the seesaw mass matrix, the mixing $V_{\nu N}$ turns out to be $\lesssim 10^{-6}$ [cf. Eq. (23)]. So the width $\Gamma(H_3 \rightarrow \nu\nu) \propto V_{\nu N}^4$ is completely negligible.

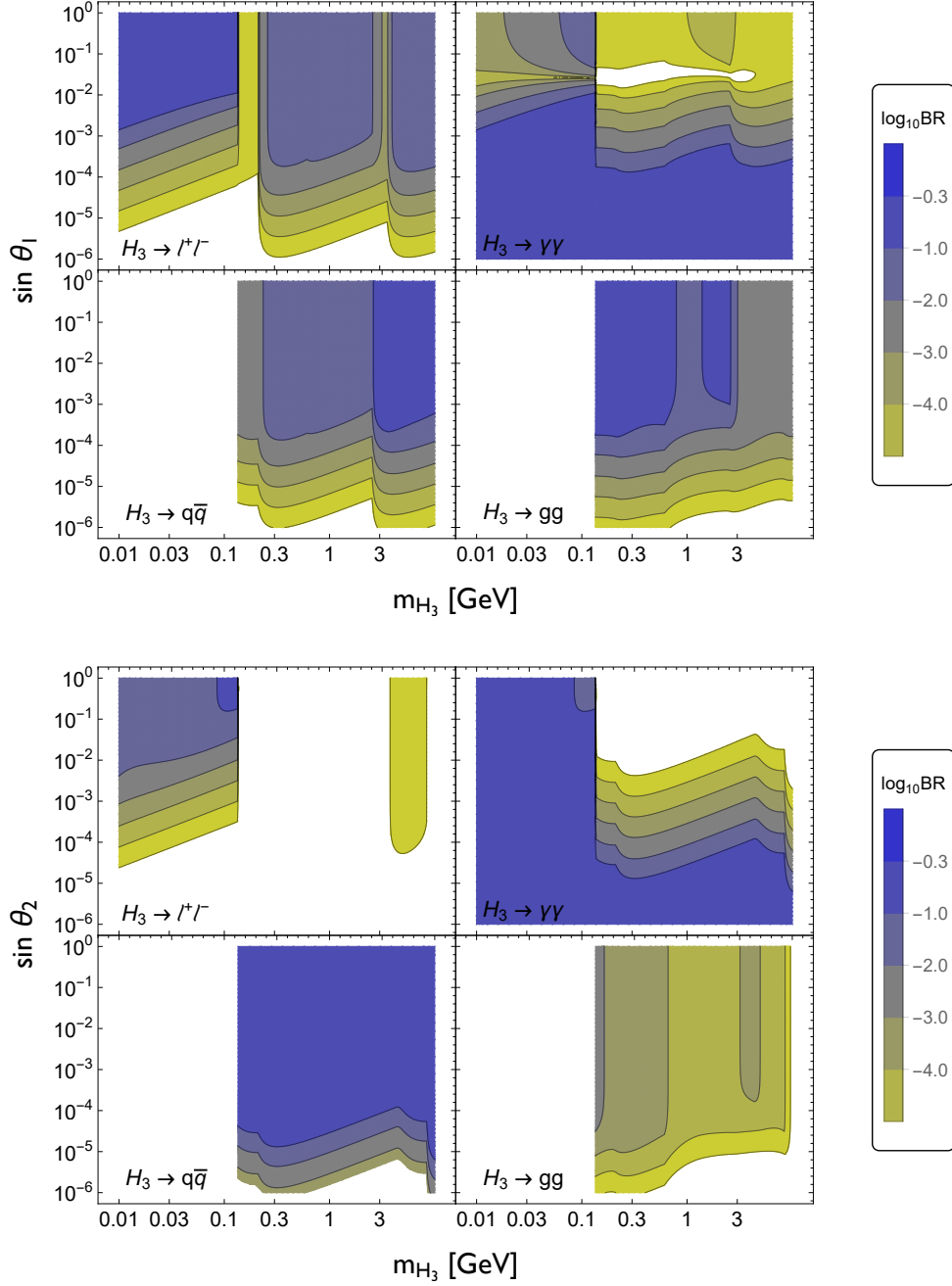


Figure 3: Color-coded branching ratios of H_3 as functions of its mass and mixing with h (top) and H_1 (bottom) for different decay modes. Here we have set the RH scale $v_R = 5$ TeV and the RHN masses at 1 TeV.

pushes the couplings $Y_{\nu N}$ to be very small, of order 10^{-7} [cf. Eq. (23)]. Furthermore, when the H_3 mass is below the pion mass, its decay to both the quark and gluon channels are kinematically forbidden, as we do not have free hadronic states in Nature lighter than pions.

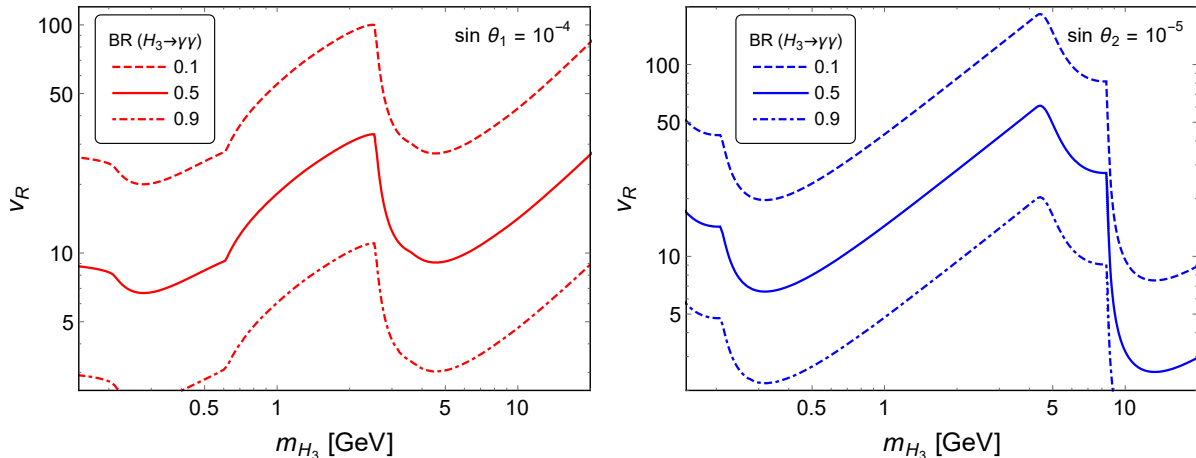


Figure 4: Contours of the $\text{BR}(H_3 \rightarrow \gamma\gamma) = 0.1, 0.5$ and 0.9 in the plane of $m_{H_3} - v_R$ for fixed value of mixing angles $\sin \theta_1 = 10^{-4}$ (left) and $\sin \theta_2 = 10^{-5}$ (right).

For these hadronic channels, the RG running of the strong coupling constant α_s is taken into consideration, which is important below the EW scale. The flavor violating decays of H_3 in both the hadronic and leptonic sectors, e.g. $H_3 \rightarrow sb, \mu\tau$, are included in making the plots in Figure 3.

From Figure 3, we find that when the mixing angles are sizable, H_3 decays mostly into the SM quarks (above the pion mass threshold) and charged leptons (below the pion mass), while when $\sin \theta_{1,2} \lesssim 10^{-4}$, the dominant decay of H_3 is into the diphoton channel, which benefits from the heavy gauge boson loops induced by the RH gauge coupling (independent of $\sin \theta_{1,2}$), with a sub-dominant contribution from the heavy scalar loops. With large BR to two photons, the FCNC constraints can be used to set limits on the mixing angles $\sin \theta_{1,2}$ as a function of m_{H_3} ; see more details in Section 5.

As shown in Figure 3, when the mixing angles $\sin \theta_{1(2)}$ are small, e.g. $\lesssim 10^{-4(5)}$, all the fermion decay modes are highly suppressed, leaving the diphoton channel as the only dominant mode. When the mixing angles become very small, the fermionic decay modes are completely negligible. In this case, the diphoton channel, being mediated by the heavy gauge and scalar bosons, depends only on the v_R scale, as mentioned above, and therefore, could probe, in principle, up to very high v_R scales, as long as the colliding energy is high enough for a sizable H_3 production cross-section through the (off-shell) heavy gauge boson mediation (see Section 6.1). To be more specific, we show in Figure 4 the contours of constant $\text{BR}(H_3 \rightarrow \gamma\gamma) = 0.1, 0.5$ and 0.9 , as a function of v_R and the light scalar mass for a fixed value of the small mixing angles $\sin \theta_1 = 10^{-4}$ (left panel) and $\sin \theta_2 = 10^{-5}$ (right panel), as enforced by the meson limits in Section 5, while the other one is set to be zero for simplicity. It is clear that the RH scale could be probed up to tens of TeV through this diphoton channel. Although such large v_R values might not be directly probed at the LHC, it could be relevant to the searches for LR seesaw at a future 100 TeV collider, such as FCC-hh or SPPC. See Section 6 for more realistic LLP searches at hadron colliders.

Using the partial decay widths given in Appendix A, we calculate the total decay length

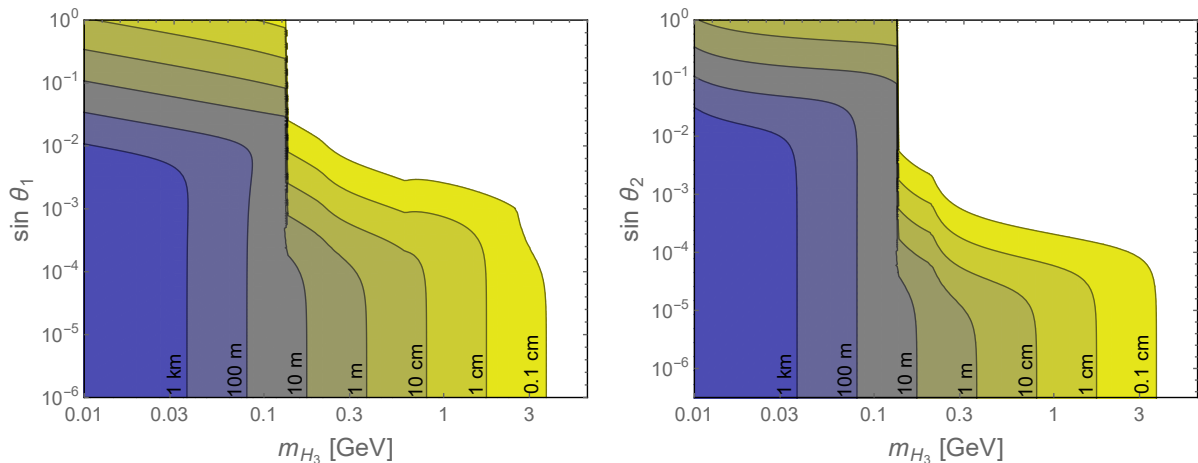


Figure 5: Contours of decay length of H_3 at rest as a function of its mass and the mixing angles $\sin\theta_{1,2}$. Here we have set the RH scale $v_R = 5$ TeV and the RHN masses at 1 TeV.

L_0 of H_3 at rest, as shown in Figure 5, as a function of its mass and mixing with h (left panel) and H_1 (right panel). From these lifetime contours, it is obvious that when the scalar H_3 mass is in the GeV range, its *proper* decay length $L_0 \sim \mathcal{O}(1)$ cm. When H_3 is produced at the LHC, it will be boosted by a Lorentz factor of $E_{H_3}/m_{H_3} \sim \mathcal{O}(100)$, so the decay length L in the laboratory frame would reach the scale of meters, thus making it a natural LLP candidate and leading to spectacular displaced vertex signals. For even smaller masses, $m_{H_3} \sim \mathcal{O}(100)$ MeV, the decay length is much longer, of order 100 m. More details of displaced vertex and LLP searches are presented in Section 6.

4. Cosmological constraints

Light particles can have an impact on the cosmological history of our Universe, depending on their decay properties. In our model, the H_3 particle is produced in the early Universe by various processes mediated by heavy scalars and gauge bosons, but at temperatures $T \ll m_{Z'}, m_{W_R}, m_h$, the dominant process that keeps H_3 in equilibrium is $\gamma\gamma \rightarrow H_3$. For a GeV-scale H_3 , it stays in equilibrium till below its mass and decouples at a lower temperature T_* , which can be estimated by equating the rate of the process $\gamma\gamma \leftrightarrow H_3$ to the Hubble expansion rate:

$$\frac{\alpha^2 T_*^3 x^{3/2} e^{-x}}{1048\pi^3} \leq \frac{10T_*^2}{M_{\text{Pl}}}, \quad (24)$$

where $x = m_{H_3}/T_*$, $\alpha \equiv e^2/4\pi$ is the fine structure constant and M_{Pl} is the Planck mass. Another relevant parameter is the decay temperature which is determined by the condition $T_d = \sqrt{\Gamma_{H_3} H(T_d)}$, where Γ_{H_3} is the total decay rate of H_3 (thermal averaged) and $H(T_d)$ is the Hubble expansion rate at temperature T_d . Typically, one requires either (i) $T_d \geq \Lambda_{\text{QCD}} \sim 150$ MeV, the QCD phase transition temperature, or (ii) $T_* \geq T_{\text{BBN}} \sim 1$ MeV, whichever is stronger, so that the primordial synthesis of light elements and the ratio of their abundances

is not affected much from their SM predicted values nor the light particle does not contribute like an extra degree of freedom at the epoch of Big Bang Nucleosynthesis (BBN). In our model, $T_d \gg T_*$ till the BBN epoch, and therefore, the condition (ii) is more stringent. Thus, we find that as long as $T_* \gtrsim 1$ MeV (or the epoch of BBN), the H_3 particle will decouple and then decay to photons which will then thermalize with the rest of the cosmic soup (e.g. by Compton scattering). This will simply reset the Hubble temperature and will not affect the cosmological history. On the other hand, if T_* is below the epoch of BBN, the H_3 particle is in equilibrium with the thermal soup and will contribute like an extra boson species and being spin zero will contribute $4/7$ to ΔN_{eff} , which is incompatible with the Planck bounds at the 2.5σ level [35]. Using Eq. (24) and setting $T_* \gtrsim 1$ MeV, we therefore obtain a conservative lower bound on $m_{H_3} \gtrsim 20$ MeV, which will be applied to our subsequent discussion.² A more accurate cosmological lower bound on m_{H_3} might be obtained by solving the relevant Boltzmann equations and calculating the temperature rise of the thermal plasma due to energy injection from the H_3 decay, but such a detailed analysis is beyond the scope of this work and might be pursued elsewhere.

5. Laboratory constraints

The light scalar H_3 mixing with the heavy flavor-changing scalar H_1 induces flavor-changing couplings of H_3 to the SM quarks and charged leptons [cf. Table 1], which are severely constrained by the low-energy flavor data, e.g. the $K^0 - \bar{K}^0$, $B_d - \bar{B}_d$ and $B_s - \bar{B}_s$ meson oscillations and rare K and B meson decays.³ In addition, the H_3 couplings are also limited by the SM invisible decay, rare top and Z boson decay, which are either absent or highly suppressed in the SM. In this section, we collect all these laboratory constraints on the $h - H_3$ and $H_1 - H_3$ mixing angles $\theta_{1,2}$, as well as their future prospects, which will provide useful guidelines for the collider searches for H_3 in the dominant $\gamma\gamma$ channel, as we will discuss in Section 6.

5.1. K and B meson oscillations

It should be emphasized that although the flavor-changing couplings of H_3 originate from the heavy scalar H_1 , the masses of H_1 and H_3 are independent observables (proportional respectively to $\sqrt{\alpha_3}$ and $\sqrt{\rho_1}$ at the leading order), therefore the constraints on H_3 derived here from flavor oscillations are different from those on the heavy scalar H_1 derived earlier in Ref. [20, 37]. Furthermore, the constraints on the mixing angles $\sin \theta_{1,2}$ from meson oscillations is sensitive to the mass of H_3 , especially when m_{H_3} is comparable to the K or B meson masses.

Taking the $K^0 - \bar{K}^0$ mixing as an explicit example, the effective four-fermion interactions mediated by H_3 can be cast into linear combinations of the effective dimension-6 operators

² H_3 masses below the supernovae core temperature of $\mathcal{O}(10$ MeV) could also be constrained from the observation of SN1987A [36].

³ The constraints from D meson sector are much weaker and thus not considered here.

of form [38]

$$\mathcal{O}_2 = [\bar{s}(1 - \gamma_5)d][\bar{s}(1 - \gamma_5)d], \quad (25)$$

$$\tilde{\mathcal{O}}_2 = [\bar{s}(1 + \gamma_5)d][\bar{s}(1 + \gamma_5)d], \quad (26)$$

$$\mathcal{O}_4 = [\bar{s}(1 - \gamma_5)d][\bar{s}(1 + \gamma_5)d]. \quad (27)$$

Though the flavor-changing couplings of H_3 to the SM fermions are from the mixing with h and H_1^0 (cf. the $\sin \tilde{\theta}_2$ terms of the Yukawa couplings in Table 1), but here they are not simply multiplied by a factor of $\sin \tilde{\theta}_2$. This is because the operators of form \mathcal{O}_2 and $\tilde{\mathcal{O}}_2$ are absent in the H_1 case, which are canceled by the CP-odd scalar A_1 in the mass degenerate limit of $m_{H_1^0} = M_{A_1^0}$. In short, the effective Lagrangian we need is

$$\begin{aligned} \mathcal{L}_{H_3} = & \frac{G_F}{4\sqrt{2}} \frac{\sin^2 \tilde{\theta}_2}{m_K^2 - m_{H_3}^2 + im_{H_3}\Gamma_{H_3}} \left[\left(\sum_i m_i \lambda_i^{RL} \right)^2 \mathcal{O}_2 + \left(\sum_i m_i \lambda_i^{LR} \right)^2 \tilde{\mathcal{O}}_2 \right. \\ & \left. + 2 \left(\sum_i m_i \lambda_i^{LR} \right) \left(\sum_i m_i \lambda_i^{RL} \right) \mathcal{O}_4 \right], \quad (28) \end{aligned}$$

where G_F is the Fermi constant, $m_i = \{m_u, m_c, m_t\}$ the running up-type quark masses, $\lambda_i^{LR} = V_{L,i2}^* V_{R,i1}$ and $\lambda_i^{RL} = V_{R,i2}^* V_{L,i1}$ the left- and right-handed quark mixing matrix elements. For simplicity we have assumed that $V_R = V_L$ which is a good approximation in the minimal LR model, up to some additional CP violating phases in the RH matrix [33, 34]. As for the heavy scalars H_1 and A_1 , the charm quark dominates the mass and quark mixing terms, i.e. $m_c \lambda$ (λ being the Cabibbo angle), with sub-leading term from the top quark $\sim m_t \lambda^5$.

To calculate the contribution of Lagrangian (28) to the $K^0 - \bar{K}^0$ mixing, we need to know the hadronic matrix elements when the operators are sandwiched by the K^0 states:

$$\langle K^0 | \mathcal{O}_i | \bar{K}^0 \rangle = N_i m_K f_K^2 B_i(\mu) R_K^2(\mu), \quad (29)$$

with $i = 2, 4$, and the K decay constant $f_K = 113$ MeV, $N_2 = 5/3$, $N_4 = -2$ and the parameters $B_2 = 0.679$, $B_4 = 0.810$ from lattice calculation [38]. The mass ratio factor $R_K = m_K / (m_d + m_s)$ is evaluated at the energy scale $\mu = 2$ GeV. As the strong interaction conserves parity, we have $\langle K^0 | \tilde{\mathcal{O}}_2 | \bar{K}^0 \rangle = \langle K^0 | \mathcal{O}_2 | \bar{K}^0 \rangle$. Then the K^0 mass difference

$$\Delta m_K \simeq 2 \text{Re} \sum_i \eta_i(\mu) \langle K^0 | \mathcal{L}_{H_3}^{(i)} | \bar{K}^0 \rangle \quad (30)$$

with $\eta_2 = 2.052$ and $\eta_4 = 3.2$ the QCD radiative corrections running from the EW scale down to the scale of $\mu \sim 2$ GeV [39].

On the experimental side, the $K^0 - \bar{K}^0$ mixing has been measured to a high accuracy, i.e. $\Delta m_K = (3.473 \pm 0.006) \times 10^{-15}$ GeV [40]; on the theoretical side, the short- and long-distance contributions to Δm_K are much larger than the experimental errors, up to 20%

of the central value. Conservatively we use 50% of the experimental central value [20] to set upper limits on the mixing angles $\sin\theta_{1,2}$, as shown in Figure 6 (blue solid lines). As expected, in the (narrow) resonance region where $m_{H_3} \simeq m_K$ the limit on the mixing angles could be largely strengthened. When the H_3 mass gets lower, the H_3 propagator is dominated by the momentum term

$$\frac{1}{q^2 - m_{H_3}^2 + im_{H_3}\Gamma_{H_3}} \rightarrow \frac{1}{q^2} \simeq \frac{1}{m_K^2}, \quad (31)$$

and the limits approach to a constant value. On the other hand, when $m_{H_3} \gg m_K$, the constraints are similar to that for the heavy scalar H_1 , and scale as $\sin\theta_{1,2}^{\text{limit}} \propto m_{H_3}$.

The calculation of flavor constraints from $B_d - \bar{B}_d$ and $B_s - \bar{B}_s$ mixings are quite similar to those from K^0 , with the QCD correction coefficient $\eta_2 = 1.654$ and $\eta_4 = 2.254$ at the B meson scale [39], and the B -parameters for the effective operators with respect to the bottom quark and d quark (or the s quark) are respectively [41]

$$\begin{aligned} B_2(B_d) &= 0.82, & B_4(B_d) &= 1.16, \\ B_2(B_s) &= 0.83, & B_4(B_s) &= 1.17. \end{aligned} \quad (32)$$

Different from the K meson case, for the $B_{d,s}$ mesons, the top quark contribution dominates in Eq. (28), which largely improves the effective coupling $\sum_i m_i \lambda_i^{LR, RL}$ and strengthens the limits on the coupling of H_3 to the bottom quark. The experimental values of $\Delta m_{B_{d,s}}$ agree well with the SM predictions [40], allowing new physics contributions of only 9.3×10^{-14} GeV and 2.7×10^{-12} GeV respectively at the 2σ level by the current CKM fitter global fit, when CP violation is neglected [42]. The corresponding upper limits on the mixing angles $\sin\theta_{1,2}$ are presented in Figure 7. The B mesons are roughly 10 times heavier than the K meson, and the absolute values of error bars for the B mass differences are much larger than Δm_K , thus the limits for the case of $m_{H_3} \lesssim m_{\text{meson}}$ is weaker for the B mixing case than that from K mixing. However, this could be partially compensated by the large effective coupling $\sum_i m_i \lambda_i^{LR, RL}$ when H_3 is heavier, especially for the B_d meson. Thus when $m_{H_3} \gtrsim m_b$, the limits on $\sin\tilde{\theta}_2$ from the B meson mixings turn out to be more stringent.

5.2. Meson decay

Since H_3 acquires flavor-changing couplings to the SM quarks via its mixing with the heavy Higgs H_1 , it could be produced from the flavor changing decay of K and B mesons, when kinematically allowed. The constraints coming from the up-sector FCNC are very weak and we do not discuss them here. In the down-type quark sector, we have the parton-level processes $b \rightarrow dH_3$, sH_3 and $s \rightarrow dH_3$ at the tree level. Depending on the mass m_{H_3} and the mixing angles $\sin\theta_{1,2}$, after being produced in K or B decays, H_3 will decay into dileptons $\ell^+\ell^-$, hadronic states $q\bar{q}$, gg , or two photons $\gamma\gamma$, with the invariant mass of the final states close to the H_3 mass. Thus, we should expect flavor-violating signals of the form

$$d_j \rightarrow d_i H_3^0, \quad \text{with } H_3 \rightarrow \text{leptons, hadrons, photons.} \quad (33)$$

The corresponding SM decay modes, like $B^+ \rightarrow K^+ \gamma \gamma$, are generally highly suppressed by the CKM matrix elements and loop factors, thus these rare decay channels are expected to set severe limits on the mixing angles $\sin \theta_{1,2}$ and hence the flavor changing couplings of H_3 to quarks.

The most stringent bounds on the decay branching ratios for the process (33) from various low-energy flavor experiments are collected in Table 2, some of which follow to some extent the discussion of Refs. [43–46]. The first simple but robust limits come from the observed total widths of K and B mesons, which depend only on the flavor-changing couplings of H_3 but not on how H_3 decays or the details of FCNC data. The lifetimes of K^\pm and K^0 are both precisely measured to the level of 10^{-3} , however the absolute theoretical values are subject to a large uncertainty of the strange quark mass, up to the order of 10% [40]. Thus, to be conservative, we take 20% of the experimental values to constrain the light scalar H_3 , which are respectively 1.33×10^{-17} GeV and 3.21×10^{-18} GeV when converted to the maximum allowed discrepancy in the total widths of K^\pm and K^0 . On the other hand, for the B meson, though the lifetime ratios such as τ_{B^\pm}/τ_{B^0} can be determined up to the level of a few %, the absolute values of τ_B are subject to large uncertainties in the form factors, at the level of 10% [40]. The 2σ lifetime uncertainties lead to an allowed discrepancy of up to 1.05×10^{-13} GeV in the total decay width of B mesons. The K and B meson width limits on $\sin \theta_{1,2}$ are shown in Figures 6 and 7 as functions of m_{H_3} . All the regions above these lines are excluded, wherein the flavor-changing decays are enhanced by the large mixing angles.

Before going into the details of other meson decay limits, let us make some general comments on the constraints from meson decays. Roughly speaking, regarding the flavor changing couplings mediated by H_3 , there are essentially two different classes of experiments that are applicable to our case. The first ones are the *visible* decays, i.e. those with visible SM particles in the final state such as $K^+ \rightarrow \pi^+ \gamma \gamma$ and $B \rightarrow K \mu^+ \mu^-$. The SM backgrounds for these rare decays are generally very small, and the tree-level flavor-changing couplings of H_3 could be severely constrained. However, the sensitivity depends largely on the selection procedure of signals, e.g. the vetoes, cuts and detector position and energy resolutions etc. The second class of processes are the *invisible* decays, i.e. the signal of type $d_j \rightarrow d_i + \text{inv.}$ at the parton level. The invisible part, or missing energy at colliders, could be from the neutrinos, such as $K^+ \rightarrow \pi^+ \nu \bar{\nu}$. We include in this category the null result of dedicated searches for a light neutral particle X^0 from meson decay, e.g. $K^+ \rightarrow \pi^+ X^0$, with the light particle long-lived enough to escape from the detector without leaving any observable footprints. These invisible decays are expected to be very sensitive to the scalar H_3 which is an LLP from the detector perspective, as long as it is light and the mixings $\sin \theta_{1,2}$ are small. In this case, we take the conservative assumption that the sensitivity depends only on the detector size but not too much on the data analysis. For these two distinct categories of searches, we use the following two branching ratios to set limits on the mixing angles $\sin \theta_{1,2}$

Table 2: Summary of meson decay constraints used to derive current/future limits on the mixing angles in Figures 6, 7 and 8. The last column gives the upper limit on the BR of the process used in our calculation. The corresponding numbers (in parenthesis) for the beam-dump experiments (last six rows) give the limit on the number of events.

Experiment	Meson decay	H_3 decay	E_{H_3}	Decay length	Limit on BR (N_{event})
NA48/2 [49]	$K^+ \rightarrow \pi^+ H_3$	$H_3 \rightarrow e^+ e^-$	~ 30 GeV	< 0.1 mm	2.63×10^{-7}
NA48/2 [50]	$K^+ \rightarrow \pi^+ H_3$	$H_3 \rightarrow \mu^+ \mu^-$	~ 30 GeV	< 0.1 mm	8.88×10^{-8}
NA62 [52]	$K^+ \rightarrow \pi^+ H_3$	$H_3 \rightarrow \gamma\gamma$	~ 37 GeV	< 0.1 mm	4.70×10^{-7}
E949 [53–56]	$K^+ \rightarrow \pi^+ H_3$	any (inv.)	~ 355 MeV	> 4 m	4×10^{-10}
NA62 [58]	$K^+ \rightarrow \pi^+ H_3$	any (inv.)	~ 37.5 GeV	> 2 m	2.4×10^{-11}
KTeV [60]	$K_L \rightarrow \pi^0 H_3$	$H_3 \rightarrow e^+ e^-$	~ 30 GeV	< 0.1 mm	2.8×10^{-10}
KTeV [61]	$K_L \rightarrow \pi^0 H_3$	$H_3 \rightarrow \mu^+ \mu^-$	~ 30 GeV	< 0.1 mm	4×10^{-10}
KTeV [62, 63]	$K_L \rightarrow \pi^0 H_3$	$H_3 \rightarrow \gamma\gamma$	~ 40 GeV	< 0.1 mm	3.71×10^{-7}
BaBar [66]	$B \rightarrow K H_3$	$H_3 \rightarrow \ell^+ \ell^-$	$\sim m_B/2$	< 0.1 mm	7.91×10^{-7}
Belle [67]	$B \rightarrow K H_3$	$H_3 \rightarrow \ell^+ \ell^-$	$\sim m_B/2$	< 0.1 mm	4.87×10^{-7}
LHCb [68]	$B^+ \rightarrow K^+ H_3$	$H_3 \rightarrow \mu^+ \mu^-$	~ 150 GeV	< 0.1 mm	4.61×10^{-7}
BaBar [73]	$B \rightarrow K H_3$	any (inv.)	$\sim m_B/2$	> 3.5 m	3.2×10^{-5}
Belle II [70]	$B \rightarrow K H_3$	any (inv.)	$\sim m_B/2$	> 3 m	4.1×10^{-6}
LHCb [76]	$B_s \rightarrow \mu\mu$	–	–	–	2.51×10^{-9}
BaBar [80]	$B_d \rightarrow \gamma\gamma$	–	–	–	3.3×10^{-7}
Belle [81]	$B_s \rightarrow \gamma\gamma$	–	–	–	3.1×10^{-6}
BaBar [84]	$\Upsilon \rightarrow \gamma H_3$	$H_3 \rightarrow qq, gg$	$\sim m_\Upsilon/2$	< 3.5 m	$[1, 80] \times 10^{-6}$
CHARM [87]	$K \rightarrow \pi H_3$	$H_3 \rightarrow \gamma\gamma$	~ 10 GeV	[480, 515] m	(< 2.3)
CHARM [87]	$B \rightarrow X_s H_3$	$H_3 \rightarrow \gamma\gamma$	~ 10 GeV	[480, 515] m	(< 2.3)
SHiP [88]	$K \rightarrow \pi H_3$	$H_3 \rightarrow \gamma\gamma$	~ 25 GeV	[70, 125] m	(< 3)
SHiP [88]	$B \rightarrow X_s H_3$	$H_3 \rightarrow \gamma\gamma$	~ 25 GeV	[70, 125] m	(< 3)
DUNE [89]	$K \rightarrow \pi H_3$	$H_3 \rightarrow \gamma\gamma$	~ 12 GeV	[500, 507] m	(< 3)
DUNE [89]	$B \rightarrow X_s H_3$	$H_3 \rightarrow \gamma\gamma$	~ 12 GeV	[500, 507] m	(< 3)

and m_{H_3} :

$$\text{visible : } \quad \text{BR}(d_j \rightarrow d_i H_3) \text{BR}(H_3 \rightarrow \chi\chi) \left[\exp\left(-\frac{L\Gamma_{H_3}}{b}\right) - \exp\left(-\frac{(L + \Delta L)\Gamma_{H_3}}{b}\right) \right], \quad (34)$$

$$\text{invisible : } \quad \text{BR}(d_j \rightarrow d_i H_3) \exp\left(-\frac{R\Gamma_{H_3}}{b}\right), \quad (35)$$

where $\chi\chi = \ell^+\ell^-$, hadrons and $\gamma\gamma$ are the visible SM particles, b is the Lorentz boost factor, L and ΔL denote respectively the distance from the primary production vertex and the decay length when H_3 decays into visible particles in the detector, and R denotes the detector size in the invisible final state case. The two different search strategies are largely complementary to each other, when applied to constrain the light scalar H_3 in the LR model.

5.2.1. K meson decay

The partial width for the charged K meson decay is given by [45, 46]

$$\Gamma(K^\pm \rightarrow \pi^\pm H_3) = \frac{G_F m_{K^\pm} \sin^2 \tilde{\theta}_2}{8\sqrt{2}\pi} \left| \sum_i m_i \lambda_{i,21}^{RL} \right|^2 \left(1 - \frac{m_{\pi^\pm}^2}{m_{K^\pm}^2} \right)^2, \quad (36)$$

where the kinetic function β_2 is defined in Eq. (A.5). For a CP-even scalar, the decay width for the neutral K meson, i.e. $K_L \rightarrow \pi^0 H_3$ is related to the charged counterpart by taking the real part of the amplitude in Eq. (36) [47].

The $\text{BR}(K^+ \rightarrow \pi^+ e^+ e^-)$ and $\text{BR}(K^+ \rightarrow \pi^+ \mu^+ \mu^-)$ are predicted to be respectively $(3.9 \pm 0.8) \times 10^{-7}$ and $(1.2 \pm 0.3) \times 10^{-7}$ in the SM [48]. Taking the largest discrepancy of the theoretical and experimental values from NA48/2 [49, 50] at the 2σ C.L., we obtain the maximum allowed contribution from potential beyond SM physics, which are listed in the last column of Table 2. Regarding the rare kaon decay with two photons in the final state, i.e. $K^+ \rightarrow \pi^+ \gamma \gamma$, we adopt the SM prediction of $(9.66 \pm 3.43) \times 10^{-7}$ with the invariant mass of diphoton $(m_{\gamma\gamma}/m_K)^2 > 0.2$ [51]. Comparing it to the measurement at NA62 [52], we arrive at the BR limit of 4.70×10^{-7} at 2σ C.L.

The kaon beam energy at NA48/2 is around $E_{\text{NA}} \simeq 60$ GeV or slightly higher, which leads to a large boost factor of $b \simeq E_{\text{NA}}/2m_{H_3}$ in Eq. (34). The position resolution of the detector could reach up to $\lesssim 1$ mm; if the LLP H_3 were produced in these experiments, the signal would be very different from the SM processes: i.e. there would be displaced ee , $\mu\mu$ or $\gamma\gamma$ tracks from the primary kaon vertex, which could be easily identified in the detector layers. To be concrete, we adopt a smaller decay length of $\Delta L = 0.1$ mm, which is more conservative than in Refs. [44, 46]. Compared to the invisible decays with H_3 leaving no trace in the detector, the visible searches are more sensitive to shorter-lived H_3 with larger mixing angles $\sin\theta_{1,2}$. The excluded regions from $K^+ \rightarrow \pi^+ \ell\bar{\ell}$ are presented in the plots of Figure 6.

In the invisible searches, the most stringent bounds are from the process $K^+ \rightarrow \pi^+ \nu\bar{\nu}$ in the experiment E949 [53–56], with neutrinos in the final state. In calculation of the limits using Eq. (35), we set $E_K \simeq 710$ MeV [57], adopt conservatively the decay length $L = 4$ m [45]⁴, and use the BR limits of 4×10^{-10} [53–55] to set separate limits on $\sin\theta_1$ and $\sin\theta_2$ by setting the other to be zero, as functions of H_3 mass, as shown in Figure 6. When m_{H_3} is close to m_π , we adopt the limit from $K^+ \rightarrow \pi^+ \pi^0$ with $\pi^0 \rightarrow \nu\bar{\nu}$ [56], which is less constraining, with the BR up to 6×10^{-8} .

The limits from $K^+ \rightarrow \pi^+ \nu\bar{\nu}$ is expected to be more stringent at the proposed running of NA62 [58], with a precision up to 10% of the SM value [58]. The theoretical uncertainty is below 4% [59], thus we take the expected largest 2σ total uncertainties $2 \times (0.10 + 0.04) \times 8.4 \times 10^{-11} = 2.35 \times 10^{-11}$ as the expected NA62 limit to constrain the couplings of H_3 , assuming the measurement of NA62 agrees well with the SM prediction.

The rare decays of neutral kaon $K_L \rightarrow \pi^0 \chi\chi$ have been searched for at the KTeV experiment, with lepton pairs $\chi\chi = e^+e^-, \mu^+\mu^-$ [60, 61] or diphoton $\gamma\gamma$ [62] in the final state.

⁴ A smaller decay length will make the constraints more stringent, see Ref. [44].

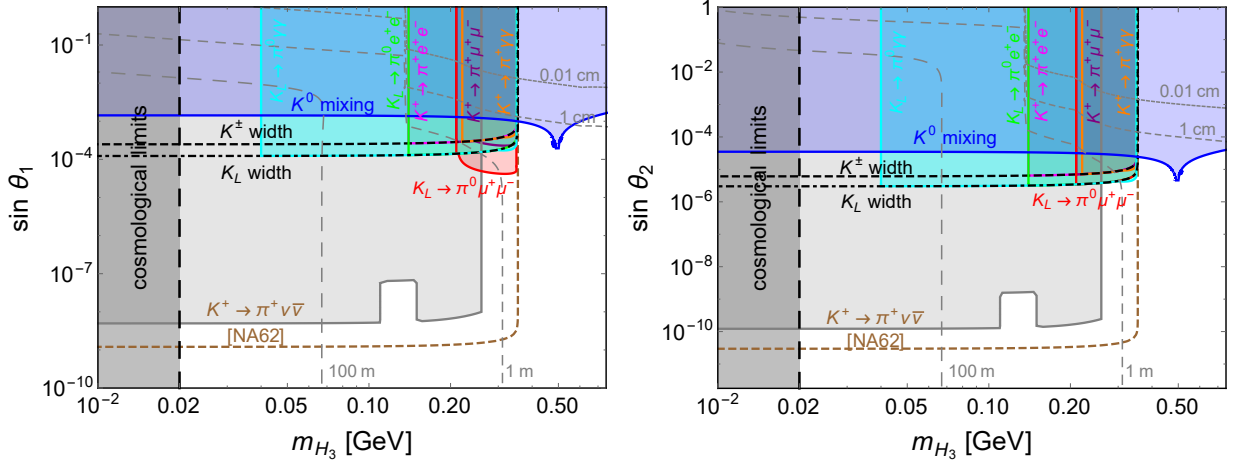


Figure 6: Flavor changing limits on the mixing angles $\sin \theta_{1,2}$ and m_{H_3} from $K - \bar{K}$ mixing (blue) and various charged and neutral kaon decay modes: $K^\pm \rightarrow \pi^\pm \chi\chi$, in the final state of leptons $\chi\chi = e^+e^-$ [49], $\mu^+\mu^-$ [50] or $\gamma\gamma$ [52] in the NA48/2 and NA62 experiments, and $K_L \rightarrow \pi^0 \chi\chi$, in the final state of leptons $\chi\chi = e^+e^-$ [60], $\mu^+\mu^-$ [61] or $\gamma\gamma$ [62, 63] in the KTeV experiment. The invisible limits from $K^\pm \rightarrow \pi^\pm \nu\bar{\nu}$ is from the E949 experiment [53–56]. The dashed brown curve is the expected sensitivity from NA62 [58]. The dashed (dot-dashed) black curve is the limit from the total K^\pm (K_L) width, whereas $m_{H_3} \lesssim 20$ MeV (vertical black-shaded) is disfavored from BBN considerations (cf. Section 4). The dashed gray lines are the *proper* lifetime of H_3 with values of 0.01 cm, 1 cm, 1 m, and 100 m. See text for more details.

The BRs are constrained to be very small, especially for the dileptons. Similar to the visible K^\pm decay at NA48/2 and NA62, the kaon system is highly boosted, with a total energy ranging from 20 GeV to 220 GeV for the dilepton searches, and 40 GeV to 160 GeV for the diphoton decay. Examining the energy distribution, we take the mean energy to be 30 and 40 GeV for the kaon system. Assuming a decay length of $\Delta L = 1$ mm, we get the visible decay limits as shown in Figure 6. Around the π^0 mass, due to the resonance effect, the SM production rate of $K_L \rightarrow \pi^0 \pi^0$ is much larger than elsewhere, and we use the SM BR($K_L \rightarrow \pi^0 \pi^0$) = 9×10^{-4} to set limits on H_3 [63].

5.2.2. B meson decay

The partial width for the exclusive B meson decay is very similar to that for K meson [cf. Eq. (36)]:

$$\Gamma(B \rightarrow KH_3) = \frac{G_F m_B \sin^2 \tilde{\theta}_2}{8\sqrt{2}\pi} \left| \sum_i m_i \lambda_{i,32}^{RL} \right|^2 \left(1 - \frac{m_K^2}{m_B^2} \right)^2 \left[f_0^{(K)}(m_{H_3}^2) \right]^2 \times \beta_2(m_B, m_K, m_{H_3}), \quad (37)$$

where $f_0(q^2)$ is a form factor of the form [64]

$$f_0(q^2) = \frac{r^2}{1 - q^2/m_{\text{fit}}^2}, \quad (38)$$

where for the K meson final state, the parameters are $r_2 = 0.330$ and $m_{\text{fit}}^2 = 37.46 \text{ GeV}^2$. For the inclusive B decays, we have

$$\Gamma(B \rightarrow X_s H_3) = \frac{G_F m_B \sin^2 \tilde{\theta}_2}{4\sqrt{2}\pi} \left| \sum_i m_i \lambda_{i,32}^{RL} \right|^2 \left(1 - \frac{m_{H_3}^2}{m_B^2} \right)^2, \quad (39)$$

with X_s standing for any strange-flavored meson.

In the SM, the BR of flavor changing decay $B \rightarrow K \ell^+ \ell^-$ ($\ell = e, \mu$) is predicted to be 5.7×10^{-7} , with large uncertainties from the form factor, top quark mass etc, summing up to 35% [65]. Comparing the theoretical prediction to the measurements at BaBar ($(6.5 \pm 1.5) \times 10^{-7}$) [66], Belle ($(4.8 \pm 0.58) \times 10^{-7}$) [67], and LHCb ($(4.36 \pm 0.23) \times 10^{-7}$) [68] and taking the largest 2σ discrepancies of theoretical and experimental values, we collect the BR limits in Table 2. The three detectors all have very good spatial resolutions [69–71]; to be concrete we take $\Delta L \sim 0.1 \text{ mm}$, and setting $L = 0$ in Eq. (34) for all of them, we obtain the excluded regions shown in in Figure 7. Again, for the B mesons at LHCb, the average energy of the B meson is $E_B^{(\text{LHCb})} \sim 300 \text{ GeV}$, so we have a large boost factor. Compared to the K decays, the flavor changing coupling to b quark is largely enhanced by the factor $\sum_i m_i \lambda_{i,32}^{RL}$. When $m_{H_3} \sim m_{J/\psi}$ or $m_{\psi(2S)}$, we use the SM BRs to set limits on H_3 [40, 45]:

$$\text{BR}(B \rightarrow K J/\psi) = \text{BR}(B \rightarrow K \ell^+ \ell^-) = 5 \times 10^{-5}, \quad (40)$$

$$\text{BR}(B \rightarrow K \psi(2S)) = \text{BR}(B \rightarrow K \ell^+ \ell^-) = 5 \times 10^{-6}. \quad (41)$$

With more B mesons collected at Belle II [70], the constraints in the visible modes could be further strengthened.

A light neutral scalar has been searched for in the decay $B \rightarrow K X^0$ in the CLEO experiment [72], with an upper limit at the level of 5.3×10^{-5} . The rare decays of $B \rightarrow K \nu \bar{\nu}$ at BaBar leads to a more stringent limit: combining both the channels of $B^+ \rightarrow K^+ \nu \bar{\nu}$ and $B^0 \rightarrow K^0 \nu \bar{\nu}$, the BR is less than 3.2×10^{-5} at the 90% C.L. [73],⁵ with the SM prediction of $\text{BR}(B \rightarrow K \nu \bar{\nu}) = (4.5 \pm 0.7) \times 10^{-6}$ [74]. With a detector size of $L = 3.5 \text{ m}$ [69], we can exclude large region in the plane of $m_{H_3} - \sin \theta_{1,2}$, as shown in Figure 7. As for the visible B decays, though the absolute value of the limit on $\text{BR}(B \rightarrow K \nu \bar{\nu})$ is much smaller than that from $\text{BR}(K \rightarrow \pi \nu \bar{\nu})$, the B meson decay is comparatively enhanced by the larger flavor changing coupling of $\sum_i m_i \lambda_{i,32}$, with respect to the coupling of $\sum_i m_i \lambda_{i,21}$ for the K mesons. With a total luminosity of 50 ab^{-1} at SuperKEKB, the $B^+ \rightarrow K^+ \nu \bar{\nu}$ could be measured up to 30% of the SM BR at Belle II [70], i.e. 1.5×10^{-6} . Applied to the LR model, this means the flavor changing couplings to b quark could be more severely constrained, as demonstrated by the dashed blue lines in Figure 7.

With the flavor-changing couplings to the quarks in B mesons, H_3 could also be produced off-shell from B meson decay and then decays into light SM particles, such as the rare

⁵ There are also searches of $B \rightarrow K^* \nu \bar{\nu}$ [70, 73], but the limits are comparatively less constraining, thus we consider here only the K mesons in the final state.

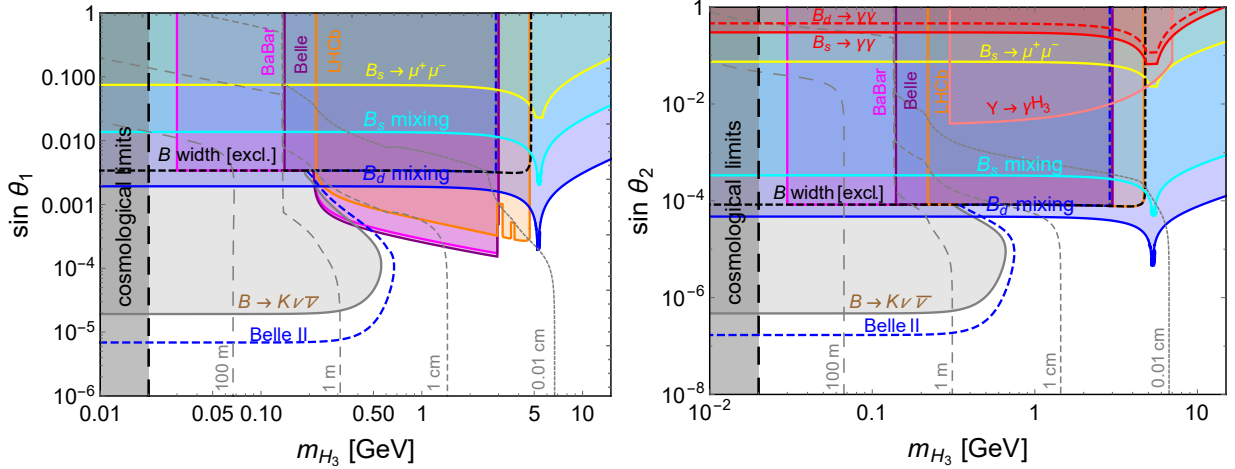


Figure 7: Flavor changing limits on the mixing angles $\sin \theta_{1,2}$ and m_{H_3} from $B_d - \bar{B}_d$ (blue) and $B_s - \bar{B}_s$ (cyan) mixings [40], B meson decay $B \rightarrow K\ell^+\ell^-$ at BaBar [66] and Belle [67] and $B \rightarrow K\mu^+\mu^-$ at LHCb [68]. The invisible limits from $B \rightarrow K\nu\bar{\nu}$ are from BaBar [73] and future prospects at Belle II [70]. The yellow lines are from the decay $B_s \rightarrow \mu^+\mu^-$. In the right panel, there are additional limits from the null result of searches of $B_{d,s} \rightarrow \gamma\gamma$ (red) [80, 81], as well as $\Upsilon \rightarrow \gamma H_3$ (pink) at BaBar [84]. The dashed black curve is the limit from the exclusive B decay width in Eq. (37). The future sensitivity of Belle II [70] is shown by the blue dashed curve. The vertical dashed (black) line is the cosmological limit. The dashed gray lines are the *proper* lifetime of H_3 with values of 0.01 cm, 1 cm, 1 m, and 100 m. See text for more details.

processes $B \rightarrow \gamma\gamma$ and $B_s \rightarrow \mu^+\mu^-$. The BR of the latter process is given by [75]

$$\frac{\text{BR}(B_s \rightarrow \mu^+\mu^-)}{\text{BR}(B_s \rightarrow \mu^+\mu^-)_{\text{SM}}} \simeq \frac{m_{B_s}^4 |C^S|^2}{4m_\mu^2 |C_{10}^{\text{SM}}|^2} \left(1 - \frac{4m_\mu^2}{m_{B_s}^2}\right), \quad (42)$$

where $C_{10}^{\text{SM}} = -4.103$ and

$$C^S = \frac{4\pi v_{\text{EW}} \mathcal{Y}_{E,\mu\mu} \sin \tilde{\theta}_2}{\alpha V_{tb} V_{ts}^* m_b (m_{B_s}^2 - m_{H_3}^2 + i\Gamma_{H_3} m_{H_3})} \left(\sum_i m_i \lambda_{i,32}^{RL} \right) \quad (43)$$

which is proportional to the flavor-changing coupling of H_3 to strange and bottom quarks and also the Yukawa coupling to muon.

The recent measurement of $\text{BR}(B_s \rightarrow \mu^+\mu^-)$ by LHCb is $(2.8 \pm 0.6) \times 10^{-9}$, compatible with the SM prediction of $(3.65 \pm 0.23) \times 10^{-9}$ [76], allowing a contribution of 2.51×10^{-9} at the 2σ C.L. from the H_3 mediated processes.⁶ The 2σ uncertainties are used to set limits on the mixing angles $\sin \theta_{1,2}$ as functions of m_{H_3} , as depicted by the yellow lines in Figure 7. Analogous to the case of K and B meson oscillations, when $m_{H_3} \sim m_{B_s}$ the constraints are enhanced by the resonance effect.

The rare decay $B_q \rightarrow \gamma\gamma$ is closely related to the parton-level flavor-changing process $b \rightarrow q\gamma\gamma$ ($q = d, s$), both of which are mediated by the FCNC couplings of H_3 to the

⁶ There are also searches of $B^0 \rightarrow \mu^+\mu^-$ [76, 77], which is however suppressed by the small flavor-changing coupling $\sum_i m_i \lambda_{i,31}$, as compared to the B_s decay, in our model.

quarks. There are two distinct sets of Feynman diagrams [78, 79]: the first one consists of the box diagrams with H_3 propagators for the couplings $bq\gamma\gamma$, the triangular diagrams for the trilinear coupling $bq\gamma$ and the H_3 mediated bq bilinear coupling; the second class are those with an s -channel H_3 coupled to the two photons via the fermion, scalar and gauge boson loops. It is expected that the second class of diagrams dominates, producing the partial width [78, 79]

$$\Gamma(B_q \rightarrow \gamma\gamma) = \frac{\alpha^3 m_{B_q}^5 f_{B_q}^2}{128\pi^2 s_W^2 m_W^2} \frac{|\mathcal{Y}_{d,qb}|^2}{|m_{B_q}^2 - m_{H_3}^2 + im_{H_3}\Gamma_{H_3}|^2} \times \left| \sum_f Q_f^2 N_C^f A_{1/2}(\tau_f) + \frac{v_{EW}}{v_R} \left(\frac{1}{3} + \frac{4}{3} - 7 \right) \right|^2. \quad (44)$$

where the factors of $1/3$, $4/3$ and -7 are respectively from the heavy H_1^\pm , $H_2^{\pm\pm}$ and W_R loops in the limit of $m_{H_3} \rightarrow 0$ [cf. Eq. (A.16)]. The current most stringent upper limits on $\text{BR}(B_d \rightarrow \gamma\gamma)$ and $\text{BR}(B_s \rightarrow \gamma\gamma)$ are respectively 3.3×10^{-7} from BaBar [80] and 3.1×10^{-6} from Belle [81].

Suppressed by the loop-induced $H_3\gamma\gamma$ coupling, the limits from $\text{BR}(B_q \rightarrow \gamma\gamma)$ are less stringent than the tree-level processes $d_j \rightarrow d_i H_3$ discussed above. Furthermore, the FCNC effects are dominated by the $\sin\theta_2$ couplings, thus the limits on $\sin\theta_1$ could hardly be constrained by the diphoton decays of B mesons. The limits on $\sin\theta_2$ are presented in Figure 7. Though $\text{BR}(B_s \rightarrow \gamma\gamma)$ is less constrained than that of B_d meson, it is comparatively enhanced by the larger coupling of $H_3\bar{s}b$ than $H_3\bar{d}b$, thus the former could exclude a larger region in Figure 7.

The bottomonium mesons Υ could decays into γH_3 at the tree level, triggered by the flavor-conserving coupling of H_3 to b quark. A light scalar has been searched for in the final state of $\mu^+\mu^-$ [82], $\tau^+\tau^-$ [83] and hadrons [84]. The BR can be normalized to $\text{BR}(\Upsilon \rightarrow \mu^+\mu^-)$, with

$$\frac{\text{BR}(\Upsilon \rightarrow \gamma H_3)}{\text{BR}(\Upsilon \rightarrow \mu^+\mu^-)_{\text{SM}}} = \frac{|\mathcal{Y}_{D,bb}|^2}{4\pi\alpha} \left(1 - \frac{m_{H_3}^2}{m_\Upsilon^2} \right) \mathcal{F}(m_{H_3}), \quad (45)$$

where $\mathcal{Y}_{D,bb}$ is the Yukawa coupling of H_3 to b quark, from both the $\sin\tilde{\theta}_1$ and $\sin\tilde{\theta}_2$ terms, and $\mathcal{F}(m_{H_3})$ is the QCD form factor, including relativistic corrections [45, 85]. As shown in Table 1, there is a relative minus sign between the $\sin\tilde{\theta}_1$ and $\sin\tilde{\theta}_2$ terms, thus for the specific well-motivated VEV ratio $\xi = \kappa'/\kappa = m_b/m_t$ adopted throughout this paper, the two terms proportional to $\sin\theta_1$ almost cancel with each other coincidentally,

$$\hat{Y}_{D,bb} \sin\tilde{\theta}_1 = y_b(\sin\theta_1 + \xi \sin\theta_2) = y_b \sin\theta_1 + y_t \xi^2 \sin\theta_2, \quad (46)$$

$$\left(V_L^\dagger \hat{Y}_U V_R \right)_{33} \sin\tilde{\theta}_2 \simeq y_t(\xi \sin\theta_1 + \sin\theta_2) = y_b \sin\theta_1 + y_t \sin\theta_2, \quad (47)$$

with only the contribution from mixing with the first two generations, which is suppressed by the small quark masses and CKM mixings to the 3rd generation. The $\sin\theta_2$ terms, however,

are not canceled, and the couplings of H_3 to bottom quarks are dominated by the $y_t \sin \theta_2$ term from the flavor changing part [cf. Eq. (47)]. For other small values of $\xi = \kappa'/\kappa$ not necessarily equal to m_b/m_t , we will “recover” the $y_b \sin \theta_1$ in Eqs. (46) and (47) with an $\mathcal{O}(1)$ coefficient, while the $y_t \sin \theta_2$ term will be affected only at the ξ^2 level. Consequently in this case the constraints on $\sin \theta_1$ is still weaker than $\sin \theta_2$. In this paper, we will not scan the full range of the small parameters ξ and ϵ .

Gathering both the contributions from gg and $q\bar{q}$, the BR of the hadronic channel $H_3 \rightarrow$ hadrons is generally larger than the leptonic modes, thus in Figure 7 we show only the constraint on $\sin \theta_2$ from the hadronic decay of H_3 , with the BR limits from 1×10^{-6} to 8×10^{-5} for H_3 mass ranging from ~ 300 MeV to ~ 8 GeV. Requiring that H_3 decays inside the detector with a radius of 3.5 m [69], we obtain the limits on $\sin \theta_2$ as shown on the right panel of Figure 7. Note that the form factor in Eq. (45) becomes smaller when H_3 is heavier, and the phase space also shrinks, thus the limit becomes less stringent for heavier H_3 .

5.2.3. Beam-dump experiments

With a huge number of protons on target (PoT), the proton fixed target experiments, like CHARM [87], SHiP [88] and DUNE [89], provide a unique opportunity to generate a large number of LLPs, and thus, complementary constraints to the collision experiments discussed above.⁷ In the beam dump experiments, a light H_3 could be produced from K and B meson decay via $K^+ \rightarrow \pi^+ H_3$, $K_L \rightarrow \pi^0 H_3$ and $B \rightarrow X_s H_3$. The searches for e^+e^- , $\mu^+\mu^-$ and $\gamma\gamma$ final states have been carried out at CHARM [87], but no signal event was found, which sets an upper limit of $N_{\text{event}} < 2.3$ at the 90% C.L. on the contribution from beyond SM physics, as shown in Table 2. Following Refs. [43–45], the H_3 production cross section is given by

$$\sigma_{H_3} \simeq \sigma_{pp} M_{pp} \left[\frac{1}{2} \chi_s \text{BR}(K^+ \rightarrow \pi^+ H_3) + \frac{1}{4} \chi_s \text{BR}(K^0 \rightarrow \pi^0 H_3) + \chi_b \text{BR}(B \rightarrow X_s H_3) \right], \quad (48)$$

with $\chi_s = 1/7$ and $\chi_b = 3 \times 10^{-8}$ the fractions of charm and bottom pair-production rates respectively, σ_{pp} the proton-proton cross section and M_{pp} the average hadron multiplicity. Normalized to the neutral pion yield $\sigma_{\pi^0} \simeq \sigma_{pp} M_{pp}/3$, we can predict the total number of $N_{H_3} \simeq 2.9 \times 10^{17} \sigma_{H_3}/\sigma_{\pi^0}$. Then the number of events collected by the detector turns out to be

$$N_{\text{event}} = N_{H_3} \left(\sum_{\chi=e,\mu,\gamma} \text{BR}(H_3 \rightarrow \chi\chi) \right) \left[\exp\left(-\frac{L\Gamma_{H_3}}{b}\right) - \exp\left(-\frac{(L+\Delta L)\Gamma_{H_3}}{b}\right) \right], \quad (49)$$

with $L = 480$ m, $\Delta L = 35$ m, $b = E_{H_3}/m_{H_3}$ the boost factor where $E_{H_3} \sim 10$ GeV [87]. Due to the huge number of events N_{H_3} , the mixing angles $\sin \theta_{1,2}$ are expected to be severely

⁷ The muon beam dump experiment could in principle be used to produce H_3 from bremsstrahlung processes [86], however, this is suppressed by the small Yukawa couplings of muon in the SM.

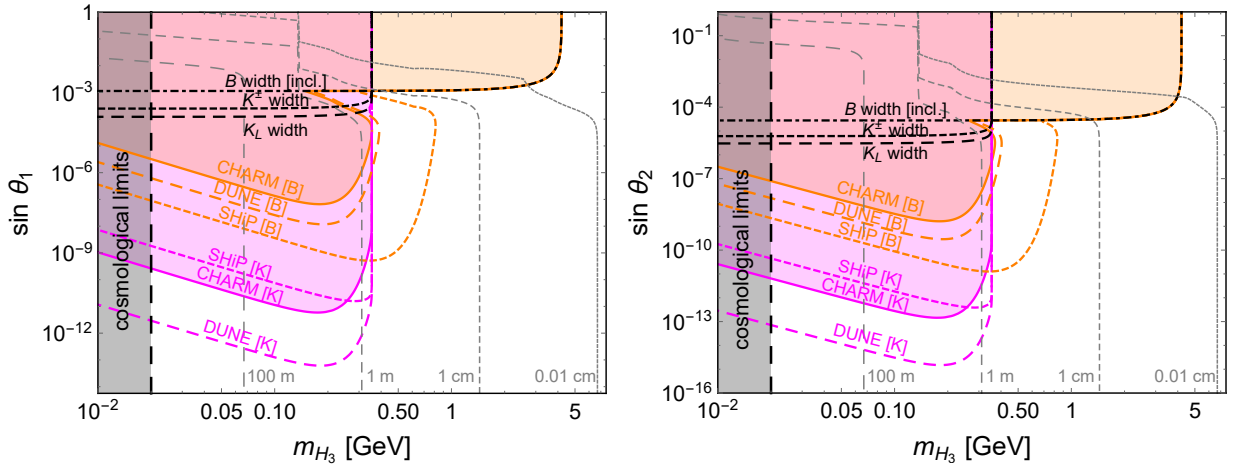


Figure 8: Limits on the mixing angles $\sin \theta_{1,2}$ and m_{H_3} from the proton beam dump experiment CHARM [87] and the future prospects at SHiP [88] and DUNE [89], in the flavor-changing decays of $K \rightarrow \pi\gamma\gamma$ and $B \rightarrow X_s\gamma\gamma$. For comparison, we also show the limits from the total width of K and inclusive B decays. The vertical black dashed line shows the cosmological limit. The dashed gray lines are the *proper* lifetime of H_3 with values of 0.01 cm, 1 cm, 1 m, and 100 m. See text for more details.

constrained, which implies that the most stringent limits are from the $\gamma\gamma$ channel, since this is the dominant decay mode of H_3 for small mixing [cf. Figure 3]. Indeed, the $\gamma\gamma$ limits from CHARM are much stronger than the meson decay limits discussed above, especially those from the kaon decays, and could reach $\sim 10^{-11}$ for both $\sin \theta_1$ and $\sin \theta_2$, as shown in Figure 8. For lighter H_3 , the boost factor b becomes larger, and fewer H_3 decays inside the detector, thus the constraints get much weaker.

Regarding the future SHiP experiment [88], it is quite analogous to CHARM but with a PoT number of 2×10^{20} . There, we could collect 8×10^{18} kaon and 7×10^{13} B meson events. With $E_{H_3} \sim 25$ GeV, $L = 70$ m, $\Delta L = 55$ m and $N_{\text{event}} < 3$, the most stringent constraints possible are also from the $H_3 \rightarrow \gamma\gamma$ decay mode. As shown in Figure 8, the K decay limits overlap largely with those from CHARM, while the B limits could be largely improved and broadened.

As for the DUNE experiment [89], with an even larger PoT of 5×10^{21} , we can collect more kaons at the near detector upstream 500 m away from the source. The total kaon number can be estimated as $N_K \simeq N_{\text{PoT}} M_{pp} \chi_s \sim 8 \times 10^{21}$ [90] with the multiplicity $M_{pp} = 11$ and $\chi_s = 1/7$ for DUNE. This could largely improve the CHARM limits by about two orders of magnitude; see Figure 8. With a small $\chi_b = 10^{-10}$ [90], the number of B mesons is much less and the expected limits from this are much weaker in Figure 8. The limits from D meson decays will be somewhat intermediate and we do not show them here.

5.3. SM Higgs, Z and top decays

The existence of a light H_3 could induce some rare or unusual decay modes for the heavier SM particles, e.g. the t quark, the Higgs and EW gauge bosons. Thus the couplings of H_3 could be limited from the relevant observations of these rare decays. Firstly, the $h - H_3$

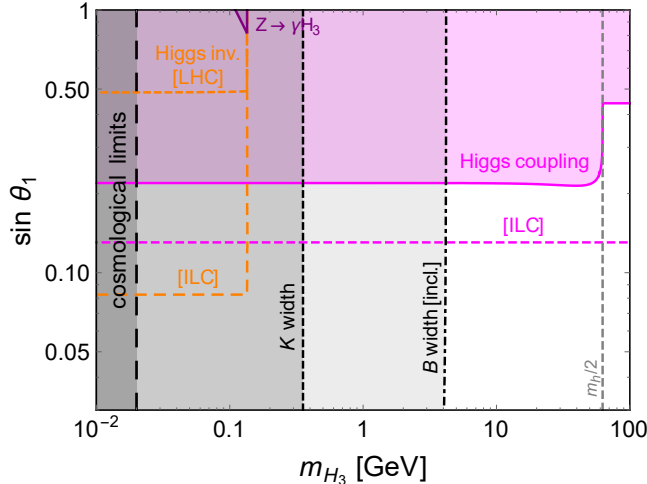


Figure 9: Limits on the mixing angle $\sin \theta_1$ as a function of m_{H_3} from precision measurements at the LHC (magenta solid) [91] and future prospects at ILC (magenta dashed) [92], as well as the limits from the invisible decay of SM Higgs by the $\sqrt{s} = 14$ TeV LHC (orange, small-dashed) [93] and $\sqrt{s} = 1$ TeV ILC (orange, dashed) [94] data, when $m_{H_3} < m_h/2$. The small purple region is excluded by searches of rare $Z \rightarrow \gamma H_3$ decay [95]. The dashed and dot-dashed black curves are the total width limit from the K and inclusive B decays. The region below 20 MeV is cosmologically disfavored. See text for more details.

mixing could rescale all the SM Higgs couplings universally. The current precision Higgs measurements at the LHC constrain a generic scalar mixing $\sin \theta_1 < 0.22$ [91], which is almost a constant for $m_{H_3} < m_h/2$. Future more precise measurements could significantly improve this up to 0.13 [92]. When $m_{H_3} < m_h/2$, we have the extra scalar decay mode for the SM Higgs,

$$\Gamma(h \rightarrow H_3 H_3) = \frac{m_h^3 \sin^2 \theta_1}{16\pi v_R^2} \sqrt{1 - \frac{4m_{H_3}^2}{m_h^2}}. \quad (50)$$

If H_3 is long-lived enough to escape the detector without leaving any signal, then it contributes to the invisible decay width of the SM Higgs. At the $\sqrt{s} = 14$ TeV LHC, with an integrated luminosity of 300 fb^{-1} , the Higgs invisible BR can be constrained to be smaller than 9% at the 95% C.L. [93], while at $\sqrt{s} = 1$ TeV ILC with a luminosity of 1000 fb^{-1} , the BR limit can reach up to 0.26% [94]. The corresponding limits on $\sin \theta_1$ are respectively 0.49 and 0.083. The Higgs coupling and invisible decay constraints on $\sin \theta_1$ are summarized in Figure 9, as solid/dashed magenta and orange lines respectively.

When $m_{H_3} < m_Z$, we have the rare Z decay $Z \rightarrow \gamma H_3$ at one-loop level mediated by mixing with the SM Higgs, with the partial width $\Gamma(Z \rightarrow \gamma H_3)$ given in Appendix B. With H_3 decaying into two photons, we would have the three-photon final states $Z \rightarrow \gamma H_3 \rightarrow 3\gamma$. However, if $m_{H_3} \ll m_Z$, the two photons from H_3 decay are highly collimated and they can not be separated experimentally. For instance, an angular separation of 20° requires that H_3 must be above the GeV scale [95]. At LEP, the rare decay $Z \rightarrow \gamma \pi^0$ has been performed, with an upper bound of 5.2×10^{-5} on the BR [96]. But this helps to constrain the mixing

$\sin \theta_1$ only by a marginal amount, as shown close to the upper border of Figure 9, because this decay into H_3 arises at loop level, and we have set the decay length at 10 cm. With a huge number $\gtrsim 10^9$ of Z events to be collected at FCC-ee [97], the limit on $\sin \theta_1$ could be improved significantly, but it may not be able to compete with the Higgs constraints.

The flavor-changing decay of top quark into up and charm quarks, i.e. $t \rightarrow uH_3, cH_3$ with $H_3 \rightarrow \gamma\gamma$ could also be used to constrain the mixing angle θ_1 . Again for $m_{H_3} \lesssim \text{GeV}$, the photon pair can not be separated apart at the LHC, and we expect to see the signals $t \rightarrow u\gamma, c\gamma$ with collimated photon jets. The current limit of 1.3×10^{-4} (1.7×10^{-3}) for $u\gamma$ ($c\gamma$) [98], can not provide any competent limits on the mixing angles $\sin \theta_{1,2}$, which is largely due to the small CKM mixing of the third generation with the first two in the SM.

Finally, we also note that constraints from flavor changing leptonic processes such as $\mu \rightarrow 3e$, are not more stringent than the hadronic decays considered above since they necessarily involve $H_3 - H_1$ mixing as well as electron and muon Yukawa couplings, which are very small.

The most important laboratory constraints discussed in this section (i.e. those ruling out some part of the parameter space not already ruled out by others) are summarized in Figure 16, together with the collider sensitivity curves to be discussed in the next section. Here the shaded regions are all excluded. The bottom line of this summary plot is that for a GeV-scale H_3 boson in the minimal LR model, the FCNC constraints necessarily imply small $h - H_3$ and $H_1 - H_3$ mixing angles $\sin \theta_{1,2} \lesssim 10^{-4}$. This naturally makes the H_3 a good LLP candidate, with distinct displaced vertex signatures of collimated diphotons, as discussed below. This is a unique feature of the minimal LR model, not shared by either a generic $U(1)_{B-L}$ model, as we will show explicitly in Section 7, or by other new physics scenarios with a light scalar, such as NMSSM [99].

6. Production and displaced vertex searches at colliders

In this section, we discuss the production of light H_3 in high-energy proton-proton collisions, and its subsequent decay to displaced photon signatures.

6.1. Production cross section

In the minimal LR model, the scalar H_3^0 can be produced from its coupling to the heavy RH gauge bosons W_R and Z_R , as well as through its coupling to the SM Higgs [11].⁸ For a small mixing $\sin \theta_1 \lesssim 10^{-4}$ of our interest, which implies the scalar quartic coupling $\alpha_1 \simeq \lambda_1 \sin \theta_1 (v_{EW}/v_R) \lesssim 10^{-6}$ [cf. Eq. (14)], the Higgs portal can be neglected, and we focus here only on the gauge portal production, which is through the associated production with a heavy W_R boson which decays predominantly into the SM quark jets ($J = u, d, s, c, b, t$):

$$pp \rightarrow W_R^* \rightarrow W_R H_3, \quad W_R \rightarrow JJ. \quad (51)$$

⁸ There is also the production of H_3 from photon fusion $\gamma\gamma \rightarrow H_3$, mediated by the W_R and scalar loops, analogous to the diagrams in Figure 2 of Ref. [100]. However, these loop-level processes turn out to be much smaller than the direct fusion of W_R and Z_R bosons in our case.

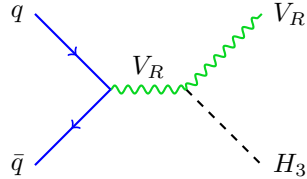


Figure 10: Production of H_3 at hadron colliders in associated production with a heavy W_R/Z_R boson.

Here for simplicity we have assumed that the decay mode into on-shell heavy RHNs $W_R \rightarrow \ell N$ is kinematically forbidden. If it is open, then we could have the smoking-gun $\ell^\pm \ell^\pm jj$ signal of the W_R boson, in association with the unique displaced photon jet from the light scalar H_3 . Other decay modes such as $W_R \rightarrow WZ, Wh$ are heavily suppressed by the small $W - W_R$ mixing angle in the minimal model we are considering [101]. One should note that the $H_3 jj$ processes (with $j = u, d, s, c$) also receive (small) contributions from the heavy vector boson fusion (VBF) $pp \rightarrow W_R^* W_R^* jj \rightarrow H_3 jj$, which is however suppressed by the three-body phase space and the off-shell W_R . At the LHC Run II, limited by the total center-of-mass energy, the associated production with the Z_R boson is always highly suppressed, as it is heavier than the W_R boson in the minimal LR scenario.

Dictated by the gauge interaction in the RH sector, the production of H_3 is only sensitive to the value of g_R ,⁹ as it determines not only the W_R mass for fixed v_R but also the magnitudes of couplings of W_R to the initial partons and H_3 . The leading order production cross sections at the $\sqrt{s} = 14$ TeV LHC for different values of $g_R/g_L = 0.6, 1, \text{ and } 1.5$ are presented in the left panel of Figure 11, where we have set the RH scale $v_R = 5$ TeV and adopted the basic trigger cuts for the jets $p_T(J) > 25$ GeV and $\Delta\phi(JJ) > 0.4$ in a `MadGraph5` set up [102].¹⁰ For a smaller $g_R < g_L$, the W_R boson is lighter and the production of H_3 can be significantly enhanced. When $m_{H_3} \lesssim 10$ GeV, the production rates are almost constant for a given v_R , and is sensitive only to the gauge coupling g_R .

6.2. Prospects at the LHC

Limited by the flavor constraints in Section 5, a light H_3 decays mostly into two photons at the LHC after being produced and flying over a distance of $L = bL_0$. For a GeV mass, the decay-at-rest length L_0 is of order of cm. The boost factor $b = E_{H_3}/m_{H_3}$ depends on the distribution of energy E_{H_3} at the LHC, which is different for different values of g_R . When the gauge coupling g_R is smaller, the W_R boson is lighter and has a larger momentum, so the scalar H_3 tends to be more highly boosted, with respect to the case with a heavier W_R . This

⁹ In the limit of $v_R \gg \sqrt{s}$, the dependence of the gauge couplings and W_R mass on the gauge coupling g_R completely cancels out, leaving only the effective dimension-seven interaction of H_3 with the SM quarks $H_3(\bar{q}_R \gamma^\mu q'_R)(\bar{q}''_R \gamma_\mu q'''_R)/v_R^3$ (note that the vertex $H_3 W_R^+ W_R^-$ is proportional to v_R , see Table 1), with the production cross section suppressed by v_R^{-6} . This is rather analogous to the W_R mediated loop contribution to the K and B meson mixing, where $m_{K,B} \ll m_{W_R}$.

¹⁰ Here for simplicity we do not distinguish the heavy flavor jets from the light quark jets from W_R decay, which are all expected to be highly boosted. The bottom and top jet tags might help to further suppress the SM background.

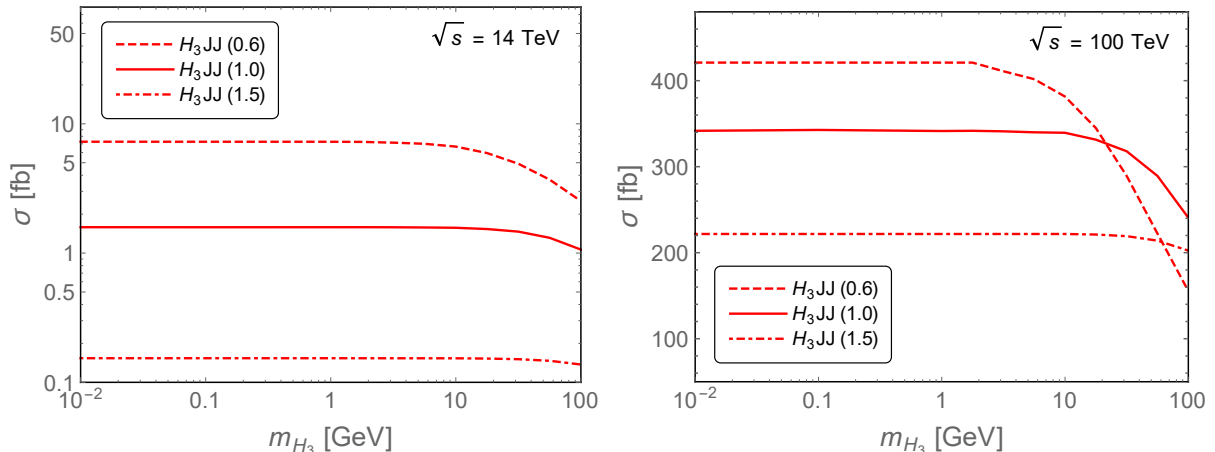


Figure 11: Production cross section of H_3 at $\sqrt{s} = 14$ TeV LHC (left) and future 100 TeV FCC-hh collider (right) in association with two quark jets, as function of its mass. The numbers in parentheses are the values of g_R/g_L . In both the plots we have set the RH scale $v_R = 5$ TeV.

effect can be seen from the energy distributions in Figure 12 from a parton-level simulation. Roughly speaking, the energy E_{H_3} has a peak at the hundred GeV scale, with a long tail up to few TeV. For our rough sensitivity estimates, we use a boost factor of order ~ 100 . Then the actual decay length is expected to be of order of meter, comparable to the radius of the Electromagnetic Calorimeter (ECAL) of ATLAS and CMS detectors, which are respectively 1.5 m [103] and 1.3 m [104, 105].

The final-state photons from H_3 decay are highly collimated with a separation of $\Delta R \sim m_{H_3}/E_{H_3}$. Thus, in a large range of parameter space, most of the photon pairs can not be separated with the angular resolution of $\Delta\eta \times \Delta\phi = 0.025 \times 0.025$ (ATLAS) and 0.0174×0.0174 (CMS) [103–105], and would be identified as a high-energy single-photon jet. Counting conservatively these single photon jets within $1 \text{ cm} < L < R_{\text{ECAL}}$, we predict the numbers of displaced diphoton events from H_3 decay in ATLAS/CMS for an integrated luminosity of 3000 fb^{-1} at $\sqrt{s} = 14$ TeV LHC – the ultimate high-luminosity phase of LHC (HL-LHC). Our results are shown in Figure 13 for three benchmark values of $g_R/g_L = 0.6, 1.0$ and 1.5 with $v_R = 5$ TeV. Here we have applied the basic trigger cuts $p_T(J) > 25$ GeV and $\Delta\phi(JJ) > 0.4$ on the jets and have assumed the SM fake rate for the displaced diphotons to be small [106–108]. We find it promising that for a GeV-scale H_3 , one could find up to $\mathcal{O}(10^4)$ displaced photon events at the LHC, which would constitute a “smoking gun” signature of the H_3 decays as predicted by the minimal LR model.

If the scalar is lighter, i.e. $m_{H_3} \lesssim 1$ GeV, the decay length would exceed the size of LHC detectors, and could be suitable for future dedicated ultra LLP (ULLP) search experiments, such as MATHUSLA [109]. Although the surface detector MATHUSLA is much farther away from the collision point, at the 100 m scale, which provides better sensitivity for low-mass LLPs, the effective solid angle of the detector being very small, at the order of $0.1 \times 4\pi$, the number of events turns out to be much smaller than those at ATLAS/CMS, as shown in Figure 13 with a high luminosity of 3000 fb^{-1} . However, the background at

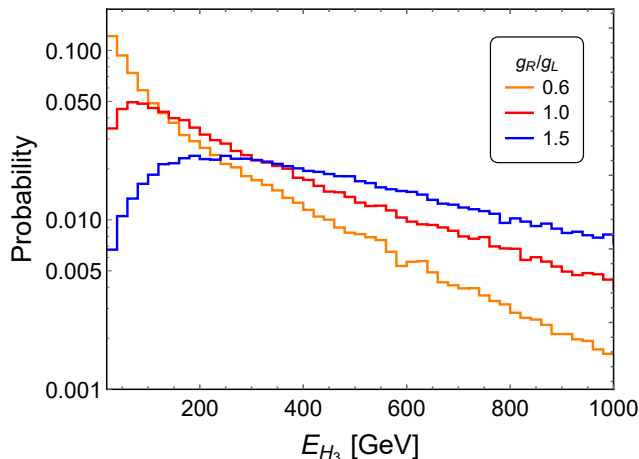


Figure 12: Energy distributions of the simulated events of H_3 production from W_R VBF, with the probability $(\frac{1}{\sigma} \frac{d\sigma}{dE_{H_3}}) \Delta E_{H_3}$ where σ is the production cross section and $\Delta E_{H_3} = 20$ GeV is the size of the energy bins considered.

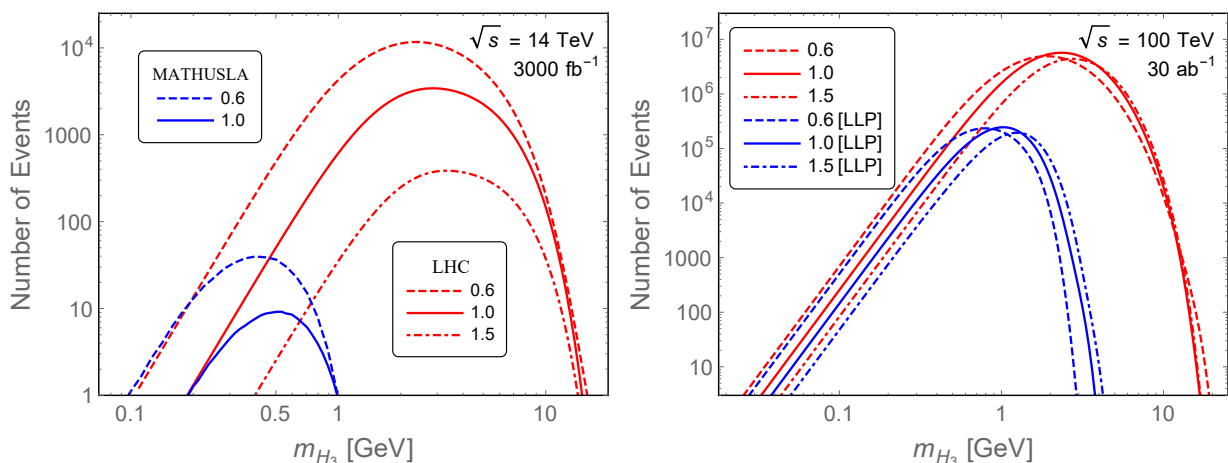


Figure 13: *Left*: Predicted numbers of displaced photon events from H_3 decay within the ECAL of ATLAS/CMS (red) and at the proposed surface detector MATHUSLA (blue), with an integrated luminosity of 3000 fb^{-1} at $\sqrt{s} = 14$ TeV, for $g_R/g_L = 0.6, 1$ and 1.5 . *Right*: The corresponding numbers of displaced photon signals at FCC-hh (red) and a forward LLP detector (blue), based on a luminosity of 30 ab^{-1} at $\sqrt{s} = 100$ TeV.

MATHUSLA is rather low or almost negligible [109, 110], whereas the displaced photon signals at ATLAS/CMS could potentially suffer from a non-negligible background, mostly from $\pi^0 \rightarrow \gamma\gamma$, which has not been considered in our preliminary analysis. Thus, we believe MATHUSLA is largely complementary to the LLP searches at ATLAS/CMS, and could extend to lower mass range of H_3 in the minimal LR model.

6.3. Prospects at future 100 TeV collider

As the physics case [111–113] for a future high-energy collider, such as FCC-hh or SPPC, with the center-of-mass energy $\sqrt{s} = 80 - 100$ TeV, is growing rapidly, we find it

worthwhile analyzing the detectable parameter space of H_3 in this scenario. The production cross section are collected in the right panel of Figure 11, where we include also the Z_R mediated processes:

$$pp \rightarrow Z_R H_3, \quad Z_R \rightarrow q\bar{q}, \ell^+ \ell^-. \quad (52)$$

We do not include the decays $Z_R \rightarrow NN$ which, depending on the RH neutrino mass, could give rise to distinct LNV signatures. Similarly, we do not consider $Z_R \rightarrow \nu\nu$, which is suppressed by the $Z - Z_R$ mixing. For the sake of comparison we retain $v_R = 5$ TeV and change only the trigger cut to $p_T(J) > 50$ GeV for the SM quark and lepton jets. For a light H_3 with mass $\lesssim 10$ GeV, the cross sections are much larger than at LHC, at the level of few 100 fb, and less sensitive to the gauge coupling g_R , as in this case the center-of-mass energy of initial partons is much larger than the W_R mass, i.e. $\hat{s} \gg M_{W_R}$, and the differences of cross section in Figure 11 is mainly due to the changes of couplings as we change g_R .

Given a ATLAS-like detector at FCC-hh, we predict the numbers of signal events at FCC-hh, with an integrated luminosity of 30 ab^{-1} of running at 100 TeV, which are shown by the red lines in the right panel of Figure 13. For concreteness, we assume the future detector has the same angular resolution as ATLAS, and count again only the highly collimated photon events, with a larger decay length ranging from $L = 10$ cm to 3 m. With a larger cross section and higher luminosity, we can collect up to 100 times more events than at the LHC. For the LR models with a larger v_R which is beyond the scope of LHC detectability, the future higher energy colliders are the only facility to study the properties of H_3 .

With a dedicated forward LLP detector at FCC-hh, similar to the one proposed in Ref. [109], the background can be significantly reduced to almost zero. With the MATHUSLA detector geometry as in Ref. [109], we obtain the numbers of signal events at the forward LLP detector, depicted as the blue lines in the right panel of Figure 13, for different values of $g_R/g_L = 0.6, 1, 1.5$.

6.4. Probing the LR seesaw model

With the expected numbers of events at LHC and MATHUSLA in Figure 13, we can easily translate them to the sensitivity regions in the plane of m_{H_3} and $\sin\theta_1$ (or $\sin\theta_2$) in the LR model, assuming that the SM background for the (ultra) LLP signal is under control. Instead of embarking on a full-fledged simulation of the detector noise for the high energy displaced photon signals, we just assume a signal number of 10 (4) at LHC (MATHUSLA) to set limits on the mass m_{H_3} and mixing angles $\sin\theta_{1,2}$ for illustration purposes. The expected sensitivity regions are shown in Figure 14, where the regions below the lines can be probed. As expected, complementary to the limits from FCNC and Higgs data in Section 5, the (U)LLP searches are sensitive to small values of mixing angles $\sin\theta_{1,2}$, as a small mixing angle would suppress the fermionic decays $H_3 \rightarrow f\bar{f}$ and ensure the dominance of $H_3 \rightarrow \gamma\gamma$ for the displaced vertex signal.

Analogously, the sensitivity regions for the LLP searches at FCC-hh and the forward detector are collected in Figure 15, where we have assumed the signal numbers to be respectively 50 and 10 for FCC-hh and the LLP forward detector. It is clearly obvious that

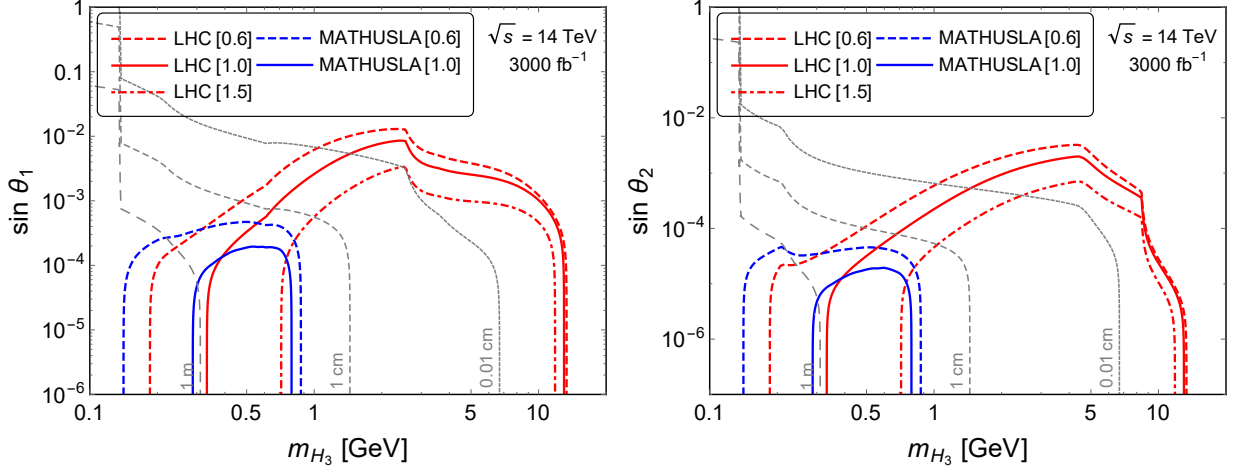


Figure 14: Sensitivity contours in the mass-mixing plane from future LLP searches at LHC and MATHUSLA, with an integrated luminosity of 3000 fb^{-1} running at $\sqrt{s} = 14 \text{ TeV}$, for $g_R/g_L = 0.6, 1$ and 1.5 . The regions below these lines are probable with 10 signal events at LHC and 4 at MATHUSLA. The dashed gray lines are the *proper* lifetime of H_3 with values of 0.01 cm, 1 cm, 1 m, and 100 m.

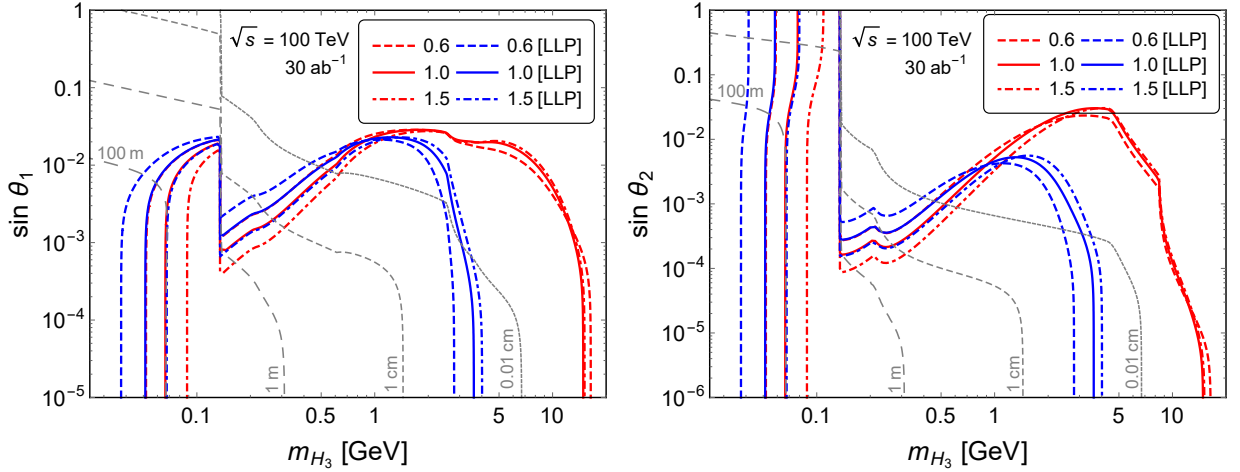


Figure 15: Sensitivity contours in the mass-mixing plane from future LLP searches at FCC-hh and forward LLP detector therein, with an integrated luminosity of 30 ab^{-1} running at $\sqrt{s} = 100 \text{ TeV}$, for $g_R/g_L = 0.6, 1$ and 1.5 . The regions below these lines are probable with 50 signal events at FCC-hh and 10 at the forward detector. The dashed gray lines are the *proper* lifetime of H_3 with values of 0.01 cm, 1 cm, 1 m, and 100 m.

compared to the regions to be probed at LHC and MATHUSLA in Figure 14, the future higher energy colliders could probe larger regions of H_3 parameter space in the minimal LR model, as well as a larger range of the gauge coupling g_R , as the H_3 production at LHC is largely limited by kinematics due to the heaviness of W_R . In the right panel of Figure 15, when the mixing angle $\sin \theta_2$ is large, e.g. $\gtrsim 10^{-2}$, and $m_{H_3} < m_\pi$ (the hadronic decays are kinematically forbidden), though $H_3 \rightarrow \gamma\gamma$ is sub-leading to the leptonic decays $H_3 \rightarrow \ell^+\ell^-$ (see Figure 3), the $\gamma\gamma$ channel is yet the dominant channel, here mediated mainly by the

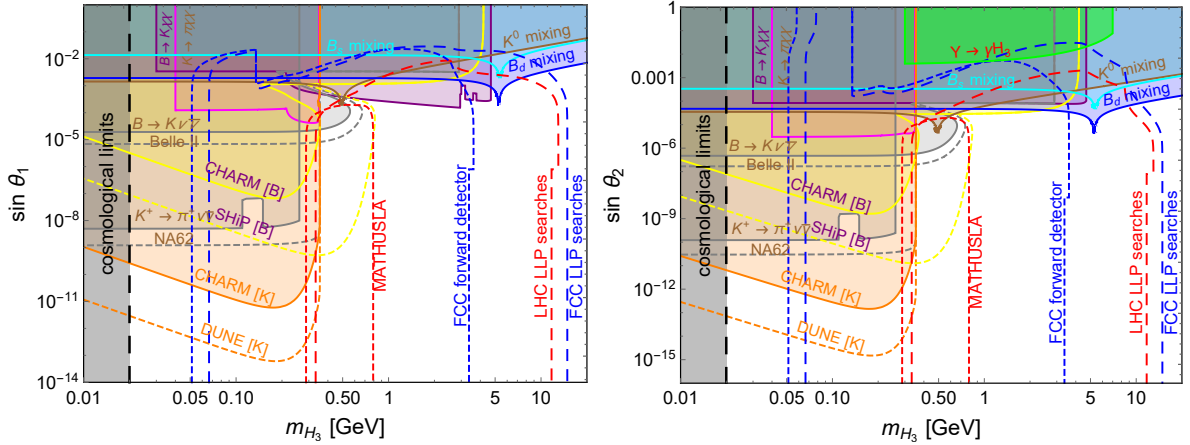


Figure 16: A summary of the important limits and sensitivity curves in the $m_{H_3} - \sin \theta_{1,2}$ plane, extracted from Figures 6, 7, 8, 14, 15. The shaded regions are excluded. For the sensitivity contours of LLP searches at LHC, MATHUSLA, FCC and the forward detector, the gauge coupling $g_R = g_L$. For details, see Sections 5 and 6.

SM fermion loops. With the huge number of signal events at both FCC-hh and the forward detector shown in Figure 13, the LLP searches can probe the mixing angle $\sin \theta_2$ up to order one, which is truly complementary to the *indirect* limits from lower energy flavor and Higgs data. This is further depicted by the summary plots in Figure 16.

From Figures 14 and 15, one might have noticed that the sensitivities become independent of $\sin \theta_{1,2}$ for very small mixing values, as the dominant contribution to the $H_3 \rightarrow \gamma\gamma$ mode only depends on the heavy gauge boson loops, and therefore, on the RH gauge coupling g_R and the RH scale v_R . Hence, it is instructive to translate the collider sensitivity regions in the $m_{H_3} - m_{W_R}$ plane by varying g_R and v_R , and assuming very small values of $\sin \theta_{1,2}$ to ensure that the $H_3 \rightarrow \gamma\gamma$ BR is almost 100%. This is shown in Figure 17 for different values of g_R/g_L . For $g_R = g_L$, we can probe m_{W_R} values up to 6 TeV or so at the LHC, which is complementary to the conventional collider searches of LR models through the same-sign dilepton plus multi-jet signal [119–132], or other collider signals in the heavy Higgs boson sector [9, 11, 30, 31, 133–140].

For completeness, we also present in Appendix C an updated sensitivity study for the displaced vertex signal in the fermion sector of the LR model, namely, from light RHN decays. Again, this probes a region complementary to those being probed by the traditional collider searches [17–19].

7. Light neutral scalar in $U(1)_{B-L}$ model

In this section, we discuss the light neutral scalar phenomenology in a simpler model based on $SU(2)_L \times U(1)_{I_{3R}} \times U(1)_{B-L}$ local symmetry. This $U(1)_{B-L}$ model can be viewed in some sense as the “effective” theory of LR model at TeV scale with the $SU(2)_R$ breaking scale and the mass of the heavy W_R bosons much higher than the TeV scale. The SM

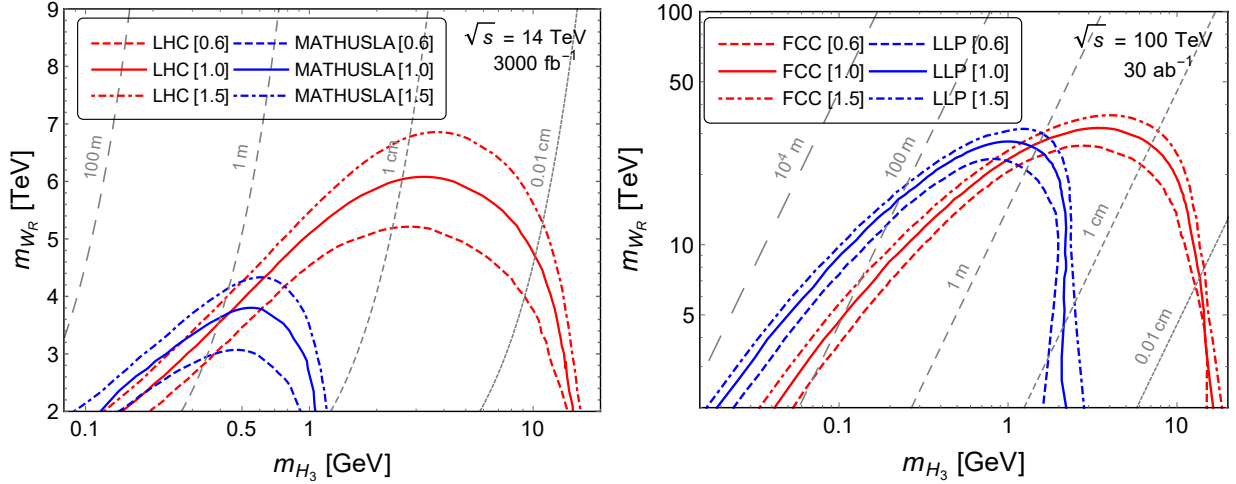


Figure 17: Collider sensitivity contours in the m_{H_3} - m_{W_R} plane from future LLP searches at LHC and FCC-hh. The grey contours indicate the proper lifetime of H_3 with $g_R = g_L$; for $g_R \neq g_L$, the lifetime has to be rescaled by the factor of $(g_R/g_L)^{-2}$.

fermions are assigned to the gauge group $SU(2)_L \times U(1)_{I_{3R}} \times U(1)_{B-L}$ as

$$\begin{aligned}
 Q &= (u_L, d_L)^T : \left(\mathbf{2}, 0, \frac{1}{3} \right); & L &= (\nu, e_L)^T : \left(\mathbf{2}, 0, -1 \right); \\
 u_R &: \left(\mathbf{1}, \frac{1}{2}, \frac{1}{3} \right); & d_R &: \left(\mathbf{1}, -\frac{1}{2}, \frac{1}{3} \right); & e_R &: \left(\mathbf{1}, -\frac{1}{2}, -1 \right).
 \end{aligned} \tag{53}$$

Anomaly freedom requires that this model has three RHNs with gauge quantum numbers $N_a : (\mathbf{1}, 1/2, -1)$. The minimal Higgs fields in the model include $H(\mathbf{2}, -1/2, 0)$ and $\Delta(\mathbf{1}, -1, 2)$ with the following Yukawa couplings:

$$\mathcal{L}_Y = h_u \bar{Q} H u_R + h_d \bar{Q} \tilde{H} d_R + h_e \bar{L} \tilde{H} e_R + h_\nu \bar{L} H N + f \bar{N}^c \Delta N + \text{H.c.} \tag{54}$$

Note that $\langle \Delta^0 \rangle = v_R$ breaks the gauge symmetry down to the SM gauge group which is further broken by $\langle H^0 \rangle = v_{EW}$ to $U(1)_{em}$. From the Yukawa interactions in Eq. (54) it is clear that after symmetry breaking this leads to the type I seesaw formula for neutrino masses. In this model, $H_3 = \text{Re}(\Delta^0)$, which mixes with the SM Higgs, governed by the angle $\sin \theta$. Different from the LR model, in the $U(1)_{B-L}$ model, we do not have the extra heavy gauge bosons, as well as the heavy doublet, which change essentially the production and decay properties of the light scalar H_3 .

7.1. Couplings and decay

The couplings of H_3 to the SM fermions are proportional to the SM Yukawa couplings, rescaled by the mixing angle $\sin \theta$, all of which are flavor conserving. However, flavor-changing coupling $H_3 \bar{s} b$ can arise at one-loop level, through the W - top loop [114]:

$$\mathcal{L}_{\text{eff}} = \frac{3\sqrt{2}G_F m_t^2 V_{ts}^* V_{tb} \sin \theta}{16\pi^2} \frac{m_b H_3 \bar{s}_L b_R}{\sqrt{2}v_{EW}} + \text{H.c.} \tag{55}$$

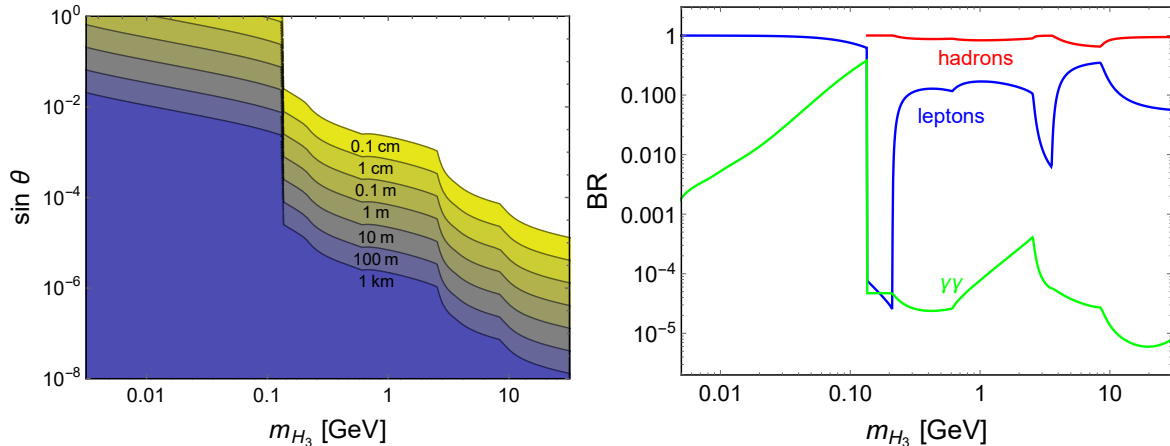


Figure 18: *Proper lifetime and branching ratios of H_3 in the $U(1)_{B-L}$ model.*

Similarly, we can have the loop-induced flavor-changing couplings to ds and db , which are all dominated by the top-quark loops.

If $m_{H_3} \lesssim \text{GeV}$, it decays predominantly into the SM fermions at tree level, and into $\gamma\gamma$ and gg at one-loop level, with the proper lifetime and branching ratios into leptons, hadrons and photons shown in Figure 5. For the hadronic modes, we combine the decays into quarks and gluons. The BRs do not depend on the mixing angle but only on H_3 mass, as all the couplings are universally proportional to the mixing angle.

7.2. Meson limits

With the loop-level flavor-changing couplings (and tree level flavor conserving couplings), we can apply the limits from K and B meson oscillations and rare decays, as for the light scalar in the LR model (see Sections 5.1 and 5.2). Compared to the LR case, the constraints are much weaker, and the most promising limits are from the lepton (ee and $\mu\mu$) and hadron decays but not the diphoton channel, which can be understood from the BR plot (Figure 18). All the limits on the mixing angle as a function of the H_3 mass are collected in Figure 19. Note that some of the limits are very weak and not shown in the plots, such as those from the total width of B mesons, the decays $B_s \rightarrow \mu\mu$ and $\Upsilon \rightarrow \gamma H_3$, and those from Higgs measurements and SM Higgs invisible decay. Comparing Figures 16 and 19, we find a new key feature that distinguishes the LR model from the $U(1)_{B-L}$ model, namely, in the former case, the meson oscillation and decay constraints rule out larger mixing angles, thus naturally ensuring the long-lived nature and diphoton decay of the light scalar, whereas in the latter case, the FCNC constraints are not so stringent, and moreover, the diphoton mode is not the dominant one.

7.3. Production and LLP searches

In the $U(1)$ model, the FCNC couplings of H_3 to the SM quarks arise at loop level; therefore, compared to the LR scenarios, the flavor limits on the mixing angle $\sin\theta$ is much weaker, as shown in Figure 19. Consequently, the light scalar H_3 could be produced either

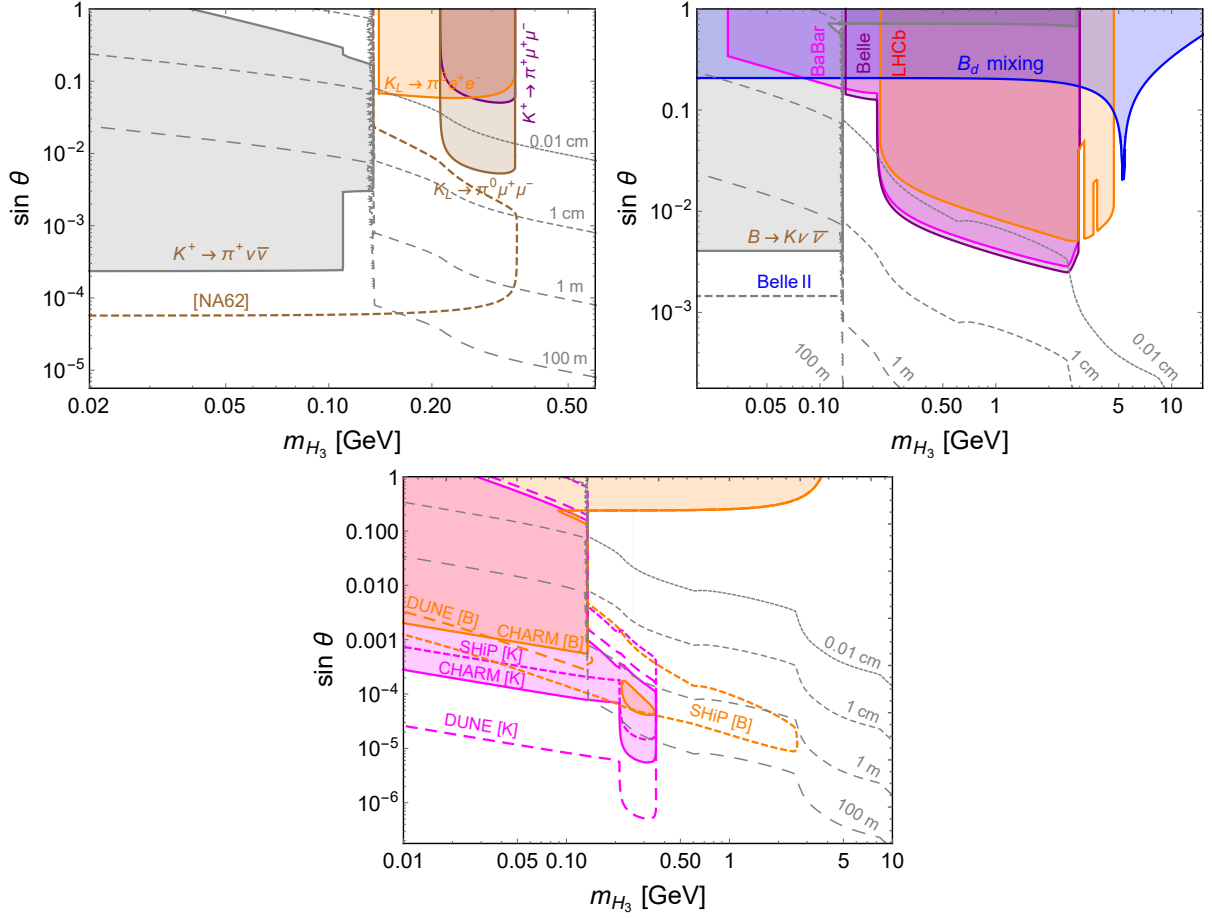


Figure 19: Limits on the light scalar mass m_{H_3} and its mixing with the SM Higgs $\sin\theta$ from the K meson decay (top, left), B meson decay and oscillation (top, right) and beam-dump experiments (bottom). The K and B_s mixing limits are very weak and not shown here.

from mixing with the SM Higgs or through the gauge interaction with the heavy Z_R boson. For a large mixing angle $\sin\theta$, the scalar H_3 could couple to the top quark, which induces an effective $H_3 gg$ coupling at the one-loop level, like the SM Higgs case. Then the dominant production mode in the scalar portal is

$$gg \rightarrow H_3 g, \quad (56)$$

at the parton-level,¹¹ with subleading contributions from the quark parton processes. When H_3 is light as we are considering, the production cross section is almost a constant,

$$\sigma(pp \rightarrow H_3 j + X) \simeq (25 \text{ pb}) \times \sin^2 \theta, \quad (57)$$

¹¹ Without the associated hard jet(s) in the final state, the light scalar H_3 is very likely to go in the beam pipe direction, which makes it hard to write such events to tape, nor could the decay products of H_3 generate any signal in the surface detector MATHUSLA.

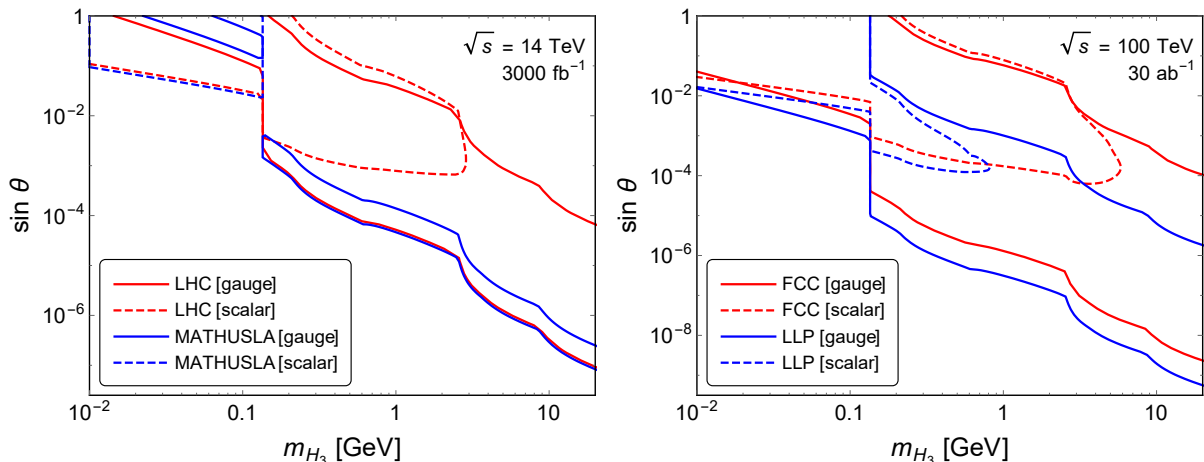


Figure 20: LLP search sensitivities at LHC, MATHUSLA (left), FCC-hh and the forward detector therein (right) in the $U(1)_{B-L}$ model, through both the gauge and scalar portals by coupling to the Z_R boson or mixing with the SM Higgs, with $g_R = 0.835g_L$. For the LHC (FCC-hh) we assume 30 (50) signal events for the hadronic decays and 10 (20) for the lepton final state, while for MATHUSLA (forward detector) we assume 4 (10) signal events.

with a conservative k -factor of 1.5, and a simple cut on the jet $p_T(j) > 50$ GeV. H_3 could also be produced via other modes, e.g. heavy VBF, whose cross sections are, however, much smaller.

With a sufficiently small m_{H_3} , i.e. lighter than the pion mass, such that H_3 could decay only into e^+e^- or $\gamma\gamma$ which are suppressed by the tiny Yukawa coupling or the loop factor, H_3 could be long-lived enough to generate displaced signals in the ATLAS/CMS detector or even at the surface detector MATHUSLA. Parton level simulations reveal that the associated jet in the final state tends to be very soft, mostly from the gluon bremsstrahlung processes, and only a small portion of the events could arrive at the MATHUSLA detector. It turns out that the dedicated LLP searches at the surface detector could yet probe a large region in the scalar portal if the mixing angle $\sin\theta > 10^{-2}$ and the scalar is lighter than roughly 100 MeV, assuming 4 signal events, as seen in Fig. 20. With more events collected by ATLAS/CMS and much shorter decay length, the displaced vertex searches at LHC could probe a much larger region as shown in Fig. 20, which is largely complementary to the ULLP searches at MATHUSLA and a cross-check in the overlapped regions.

In the gauge portal, i.e. via interaction with the Z_R boson, the dominant production mode is the associated production with a heavy Z_R boson, as in the LR models, with Z_R decaying further into the SM quarks and charged leptons (here again we do not consider the decays $Z_R \rightarrow \nu\bar{\nu}$, NN as in the LR case):

$$pp \rightarrow Z_R^* \rightarrow Z_R H_3, \quad Z_R \rightarrow q\bar{q}, \ell^+\ell^-, \quad (58)$$

with subleading contributions from the VBF of two Z_R bosons $pp \rightarrow Z_R^* Z_R^* jj \rightarrow H_3 jj$. With the heavy Z_R boson taking away most of the energy in the final state, the light scalar H_3 tends to be very soft, with a transverse momentum typically $\lesssim 100$ GeV for most of the

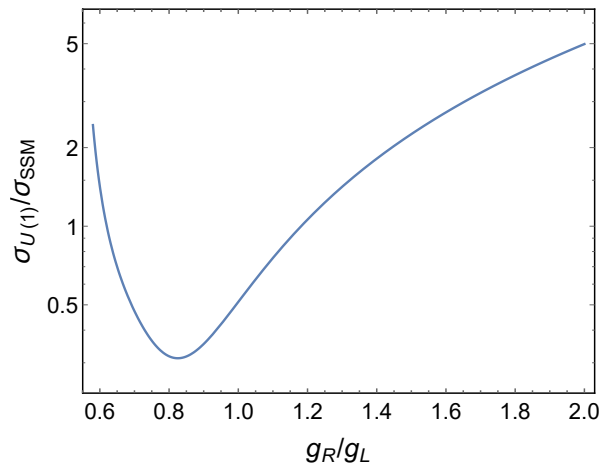


Figure 21: Production cross section of $\sigma(pp \rightarrow Z_R)$ times the branching ratio into dileptons ee and $\mu\mu$, in units of the corresponding cross section in the sequential SM.

events. Therefore only a small portion of the H_3 events could arrive at the surface detector, as in the scalar portal. With the current LHC dilepton searches [115–118], the Z_R mass is required to be above the TeV scale. Rescaling from the Z' boson in sequential SM, we get the mass limit to be 3.72 TeV with the gauge coupling $g_R = g_L$ in the $U(1)_{B-L}$ model. With a smaller $g_R = 0.835g_L$, the constraint becomes slightly less stringent, at 3.64 TeV. This is the optimistic scenario, as when g_R gets smaller, the couplings to quarks and leptons would be larger benefitting from a larger gauge coupling g_{BL} . The exact dependence of the production cross section (with respect to that in the sequential SM) with the ratio g_R/g_L is shown in Figure 21. Note that the ratio g_R/g_L is bounded from below, otherwise the $U(1)_{B-L}$ gauge coupling g_{BL} becomes non-perturbative:

$$\frac{g_R}{g_L} > \tan \theta_w \left(1 - \frac{e^2}{g_{BL}^2 \cos^2 \theta_w} \right)^{-1/2}. \quad (59)$$

With Z_R mass set at the optimistic value $g_R = 0.835g_L$, we obtain the production cross section of 0.97 fb in the gauge portal, assuming a k -factor of 1.2.

With the optimistic value $g_R = 0.835g_L$, which corresponds to the weakest limit on $m_{Z'}$ from Figure 21, and therefore, the largest H_3 production cross section at the LHC, we estimate the expected signal events at $\sqrt{s} = 14$ TeV LHC with a luminosity of 3000 fb^{-1} . Assuming the signal number of 30 for the hadronic decays and 10 for the leptonic decays, we can probe a large region in the plane of m_{H_3} and $\sin \theta$, as shown in Figure 20. Inside the region surround by the red curve, the signal number in the gauge portal could even reach up to few hundreds. The direct LLP searches at LHC are largely complementary to the indirect limits from meson oscillations and rare decays in Figure 19.

Limited by the Z_R mass limits and thus the small production cross section, the ULLP signal number at MATHUSLA could probe a narrow band in the parameter space of $m_{H_3} - \sin \theta$, as shown in Fig. 20, though the mixing angle $\sin \theta$ could be much smaller than that in the scalar portal, with the detector geometry and efficiency as given in Ref. [109]. When

g_R/g_L is different from the optimistic value of 0.835, the Z' limits from LHC become more stringent, and it is much more difficult to collect ULLP signals at MATHUSLA, irrespective of the final states being leptons or jets. However, the virtually background-free environment in the MATHUSLA detector might make it possible to probe the $U(1)_{B-L}$ model even with such small number of signal events. The prospects at a future 100 TeV collider with a dedicated forward detector is more promising for ULLP searches.

With the heavy Z_R boson more abundantly produced at the future 100 TeV collider such as FCC-hh, the probable regions of LLP searches could be significantly broadened in both the scalar and gauge portals, as presented in the right panel of Figure 20, where we have assumed 50 LLP events in the hadronic channel and 20 in the leptonic channel, and 10 events at the forward detector, with the same geometry as for the LR case. With the large production cross section, which could reach about 310 fb,¹² and the huge luminosity of 30 ab^{-1} and high center-of-mass energy, the LLP searches at future 100 TeV colliders and forward detector could probe the proper lifetime from 0.01 cm up to 10^4 m, for a wide range of H_3 mass from 10 MeV up to tens of GeV, and could even probe the mixing angle up to 10^{-9} . As in the case of LR model, due to the large boost factors in the production of H_3 at the high energy colliders, the LLP searches at LHC and future 100 TeV colliders are sensitive to the relatively higher mass range, complementary to the high intensity experiments, which is explicitly shown in Figure 22 where we collect all the important limits and prospects.

8. Conclusion

We have pointed out that, the real part of Higgs field that breaks local $B - L$ symmetry in low-scale type I seesaw models for neutrino masses can be very light with mass in the GeV to sub-GeV range. When $B - L$ is part of the left-right seesaw model, the light scalar couplings to Standard Model fields are so weak due to FCNC constraints on the model that it necessarily becomes a long-lived particle, leading to high energy displaced photons at the current LHC detectors (see the summary plots in Figure 16). Searches for them could therefore provide a new probe of the TeV scale left-right seesaw models. We have also carried out an analogous discussion for the simple $U(1)_{B-L}$ scenario. While the FCNC constraints are not so strong for this case, we show that for small mixings (or smaller H_3 masses) there can be observable displaced vertex signals (see Figure 22). We have also commented (in Appendix C) on the possibility of light right-handed neutrinos giving displaced vertices.

As clearly shown in Figure 16 and 22, the displaced vertex searches at LHC and future 100 TeV collider, no matter whether the displaced signals are the collimated diphotons, the hadronic jets or the charged leptons, are largely complementary to the probes of the oscillations and rare decays in the meson sector on the light scalar in the seesaw models. Compared to the comparatively lower-energy high intensity experiments, the high energy

¹² Here for the sake of concreteness and comparison with the LHC case we have assumed again the gauge coupling $g_R = 0.835g_L$; with other values of g_R , the production cross section could be even larger at the 100 TeV collider, though Z_R might be heavier, then the sensitivity regions in the right panel of Fig. 20 could even be larger.

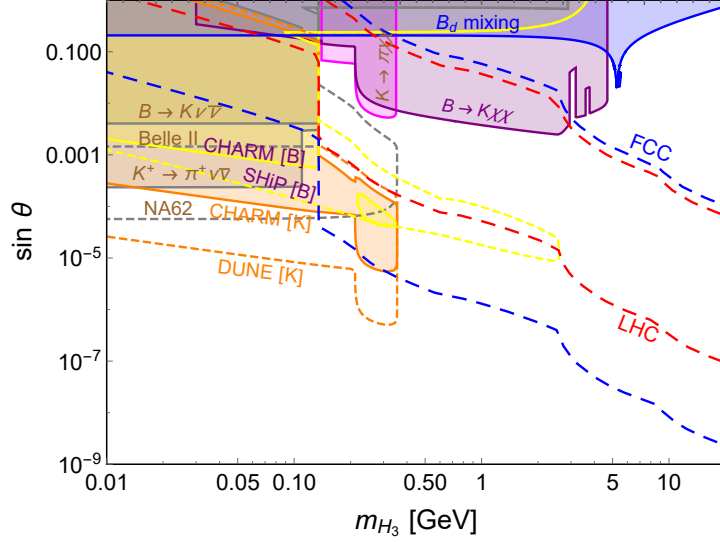


Figure 22: A summary of the important limits and sensitivity curves in the $m_{H_3} - \sin \theta$ plane in the $U(1)_{B-L}$ model, extracted from Figures 19 and 20. The shaded regions are excluded, while those surrounded by the dashed red and blue lines are the expected sensitivities in the gauge portal from LLP searches at LHC and future 100 TeV collider FCC-hh. For details, see Section 7.

frontier tends to extend the probable scalar mass to larger values, and the mixing angles to smaller values. Furthermore, both these two avenues are also complementary to the direct tests of heavy right-handed (or $U(1)_{B-L}$) sector at the hadron colliders. We believe that our work provides another window using experiments in the lifetime frontier to probe the possibility of TeV scale origin of neutrino masses.

Acknowledgments

We thank David Curtin and Brian Shuve for useful discussions and correspondence on MATHUSLA. The work of R.N.M. is supported by the US National Science Foundation grant No. PHY1620074. Y.Z. would like to thank the IISN and Belgian Science Policy (IAP VII/37) for support.

Appendix A. Partial decay widths of H_3

Here we collect all the partial widths for the dominant decay modes of H_3 :

$$\Gamma(H_3 \rightarrow q\bar{q}) = \frac{3m_{H_3}}{16\pi} \left[\sum_{i,j} |\mathcal{Y}_{u,ij}|^2 \beta_2^3(m_{H_3}, m_{u_i}, m_{u_j}) \Theta(m_{H_3} - m_{u_i} - m_{u_j}) + \sum_{i,j} |\mathcal{Y}_{d,ij}|^2 \beta_2^3(m_{H_3}, m_{d_i}, m_{d_j}) \Theta(m_{H_3} - m_{d_i} - m_{d_j}) \right] \quad (\text{A.1})$$

$$\Gamma(H_3 \rightarrow \ell^+ \ell^-) = \frac{m_{H_3}}{16\pi} \sum_{i,j} |\mathcal{Y}_{e,ij}|^2 \beta_2^3(m_{H_3}, m_{e_i}, m_{e_j}) \Theta(m_{H_3} - m_{e_i} - m_{e_j}), \quad (\text{A.2})$$

$$\Gamma(H_3 \rightarrow \gamma\gamma) = \frac{\alpha^2 m_{H_3}^3}{1028\pi^3} \left| \frac{\sqrt{2}}{v_R} A_0(\tau_{H_1^\pm}) + \frac{4\sqrt{2}}{v_R} A_0(\tau_{H_2^{\pm\pm}}) + \frac{\sqrt{2}}{v_{\text{EW}}} \sum_{f=q,\ell} f_f N_C^f Q_f A_{1/2}(\tau_f) + \frac{\sqrt{2}}{v_R} A_1(\tau_{W_R}) \right|^2, \quad (\text{A.3})$$

$$\Gamma(H_3 \rightarrow gg) = \frac{G_F \alpha_s^2 m_{H_3}^3}{36\sqrt{2}\pi^3} \left| \frac{3}{4} \sum_{f=q} f_f A_{1/2}(\tau_f) \right|^2, \quad (\text{A.4})$$

with the kinetic function

$$\beta_2(M, m_1, m_2) \equiv \left[1 - \frac{2(m_1^2 + m_2^2)}{M^2} + \frac{(m_1^2 - m_2^2)^2}{M^4} \right]^{1/2}, \quad (\text{A.5})$$

$\mathcal{Y}_{u,d,e}$ the Yukawa couplings given in Table 1,

$$\mathcal{Y}_u = \widehat{Y}_U \sin \tilde{\theta}_1 - (V_L \widehat{Y}_D V_R^\dagger) \sin \tilde{\theta}_2, \quad (\text{A.6})$$

$$\mathcal{Y}_d = \widehat{Y}_D \sin \tilde{\theta}_1 - (V_L^\dagger \widehat{Y}_U V_R) \sin \tilde{\theta}_2, \quad (\text{A.7})$$

$$\mathcal{Y}_e = \widehat{Y}_E \sin \tilde{\theta}_1 - Y_{\nu N} \sin \tilde{\theta}_2, \quad (\text{A.8})$$

f_f the normalization factor with respect to the SM Yukawa couplings,

$$f_{u,i} = \sin \tilde{\theta}_1 - \frac{(V_L \widehat{M}_d V_R^\dagger)_{ii}}{m_{u,i}} \sin \tilde{\theta}_2, \quad (\text{A.9})$$

$$f_{d,i} = \sin \tilde{\theta}_1 - \frac{(V_L^\dagger \widehat{M}_u V_R)_{ii}}{m_{d,i}} \sin \tilde{\theta}_2, \quad (\text{A.10})$$

$$f_{e,i} = \sin \tilde{\theta}_1 - \frac{Y_{\nu N,ii}}{m_{e,i}/v_{\text{EW}}} \sin \tilde{\theta}_2, \quad (\text{A.11})$$

and the loop functions

$$A_0(\tau) \equiv -[\tau - f(\tau)] \tau^{-2}, \quad (\text{A.12})$$

$$A_{1/2}(\tau) \equiv 2[\tau + (\tau - 1)f(\tau)] \tau^{-2}, \quad (\text{A.13})$$

$$A_1(\tau) \equiv -[2\tau^2 + 3\tau + 3(2\tau - 1)f(\tau)] \tau^{-2}, \quad (\text{A.14})$$

with $\tau_X = m_{H_3}^2/4m_X^2$ and

$$f(\tau) \equiv \begin{cases} \arcsin^2 \sqrt{\tau} & (\text{for } \tau \leq 1) \\ -\frac{1}{4} \left[\log \left(\frac{1+\sqrt{1-1/\tau}}{1-\sqrt{1-1/\tau}} \right) - i\pi \right]^2 & (\text{for } \tau > 1). \end{cases} \quad (\text{A.15})$$

For the heavy particle loops, only the limits below are useful for us

$$A_0(0) = 1/3, \quad A_{1/2}(0) = 4/3, \quad A_1(0) = -7. \quad (\text{A.16})$$

Thus in Eq. (A.3), we have a suppression factor of $5A_0(0)/A_1(0) = -5/21$ for scalar loops, with the factor of 5 coming from the sum of electric charges squared.

Appendix B. Rare Z decay $Z \rightarrow \gamma H_3$

The partial width of rare Z decay reads

$$\begin{aligned} \Gamma(Z \rightarrow \gamma H_3) &= \frac{G_F^2 \alpha m_W^2}{192\pi^4} m_Z^3 \left(1 - \frac{m_{H_3}^2}{m_Z^2}\right)^3 \\ &\times \left| \sin \theta_1 A_1(\tau_W, \lambda_W) + \sum_{f=q,\ell} \frac{f_f N_C^f Q_f \hat{v}_f}{c_W} A_{1/2}(\tau_f, \lambda_f) \right|^2, \end{aligned} \quad (\text{B.1})$$

with $\tau_X = 4m_X^2/m_{H_3}^2$, $\lambda_X = 4m_X^2/m_Z^2$, and the loop functions are defined as

$$A_{1/2}(\tau, \lambda) \equiv I_1(\tau, \lambda) - I_2(\tau, \lambda), \quad (\text{B.2})$$

$$A_1(\tau, \lambda) \equiv c_W \left[4 \left(3 - \frac{s_W^2}{c_W^2} \right) I_2(\tau, \lambda) + \left(\left(1 + \frac{2}{\tau} \right) \frac{s_W^2}{c_W^2} - \left(5 + \frac{2}{\tau} \right) \right) I_1(\tau, \lambda) \right], \quad (\text{B.3})$$

with

$$\begin{aligned} I_1(\tau, \lambda) &\equiv \frac{\tau\lambda}{2(\tau-\lambda)} + \frac{\tau^2\lambda^2}{2(\tau-\lambda)^2} [f(\tau^{-1}) - f(\lambda^{-1})] \\ &\quad + \frac{\tau^2\lambda}{(\tau-\lambda)^2} [g(\tau^{-1}) - g(\lambda^{-1})], \end{aligned} \quad (\text{B.4})$$

$$I_2(\tau, \lambda) \equiv -\frac{\tau\lambda}{2(\tau-\lambda)} [f(\tau^{-1}) - f(\lambda^{-1})], \quad (\text{B.5})$$

$f(x)$ as defined in Eq. (A.15), and

$$g(\tau) \equiv \begin{cases} \sqrt{\tau^{-1}-1} \arcsin \sqrt{\tau} & (\text{for } \tau \leq 1) \\ \frac{\sqrt{1-\tau^{-1}}}{2} \left[\log \left(\frac{1+\sqrt{1-1/\tau}}{1-\sqrt{1-1/\tau}} \right) - i\pi \right] & (\text{for } \tau > 1). \end{cases} \quad (\text{B.6})$$

Appendix C. Light RH neutrinos in the LR seesaw model

The RHNs have extra charged current interactions in the LR model mediated by the heavy W_R boson, which are not suppressed by the heavy-light neutrino mixings, but sensitive to the RH scale v_R (or equivalently the W_R mass, up to the gauge coupling g_R). Though the ULLP signals in this case are very similar to the light scalar case discussed in Section 6.4, i.e. highly collimated leptonic and hadronic jets, the production modes and phenomenological implications are very different.

In the LR model, the decay of RHNs are predominantly mediated by an off-shell heavy W_R boson: $N \rightarrow W_R^* \ell \rightarrow \ell jj$. When $m_N \ll m_{W_R}$ which is the case for a light RHN to be viable ULLP candidate at the LHC, the three-body decay width is given by

$$\Gamma_N \simeq \frac{3G_F^2}{32\pi^3} m_N^5 \left(\frac{m_W}{m_{W_R}} \frac{g_R}{g_L} \right)^4. \quad (\text{C.1})$$

For a few-TeV scale W_R , if the RHN mass is order 10 GeV, then its *proper* lifetime would be at the cm level:

$$\tau_N^0 \simeq 9.3 \times 10^{-3} \left(\frac{m_N}{10 \text{ GeV}} \right)^{-5} \left(\frac{m_{W_R}}{3 \text{ TeV}} \right)^4 \left(\frac{g_R}{g_L} \right)^{-4} \text{ m}. \quad (\text{C.2})$$

Such a light RHN at the GeV scale can be produced from rare meson decays, such as $D_s \rightarrow eN$ (here for simplicity we assume the RHN is of electron flavor), with the subsequent decay $N \rightarrow e\pi$ [141]. Both the production of N from mesons and decay into lighter states are mediated by its gauge interaction to the heavy W_R boson. The masses m_{W_R} , m_N and the gauge coupling g_R can thus be probed at dedicated beam dump experiments, such as SHiP [88, 141]. Here we present a sensitivity study for the displaced vertex signal at the LHC.¹³

In the minimal LR model with the $SU(2)_R$ gauge symmetry broken by the RH triplet scalar, $m_{Z_R} > m_{W_R}$. Thus the dominant production of RHNs at the LHC is through the s -channel W_R exchange: $pp \rightarrow W_R^{(*)} \rightarrow \ell N$, followed by the three-body decay $N \rightarrow W_R^* \ell \rightarrow \ell jj$ [119]. With $m_{W_R} \gtrsim 3 \text{ TeV} (g_R/g_L)^4$, as required to satisfy the direct LHC constraints [17–19], as well as the low-energy FCNC constraints [20], the production cross section could reach few tens of fb, depending on the W_R mass as well as the gauge coupling g_R . Here we have imposed the condition that the associated lepton (jet) must satisfy the basic trigger cuts of $p_T > 25 \text{ GeV}$ and $|\eta| < 2.5$. Requiring that the decay length $1 \text{ cm} < L_N < 1.5 \text{ m}$ with the ECAL size of the ATLAS detector, we obtain the sensitivity reach for light RHN as shown in Figure C.23 for three different values of the gauge coupling $g_R/g_L = 0.6, 1$ and 1.5 at the $\sqrt{s} = 14 \text{ TeV}$ HL-LHC with an integrated luminosity of 3000 fb^{-1} . For concreteness, we have assumed only the electron flavor $\ell = e$ without RH leptonic mixing, and the number of signal

¹³ In the minimal type I seesaw model without the LR symmetry, the small Yukawa couplings of the RHNs also make them long-lived with displaced vertex signatures at colliders [142, 143]; however, their production cross section will also be suppressed by the same Yukawa couplings.

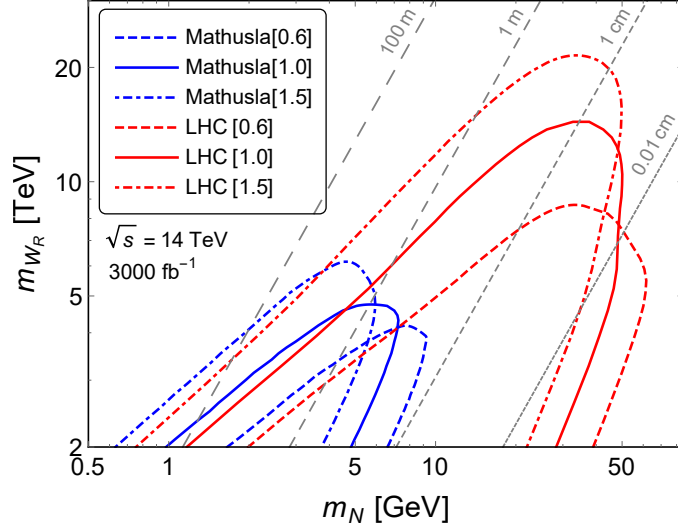


Figure C.23: Light RHN sensitivity in the minimal LR model from the ULLP searches at the $\sqrt{s} = 14$ TeV LHC (red) and MATHUSLA (blue) for three different values of $g_R/g_L = 0.6, 1$ and 1.5 . The grey contours indicate the proper decay length of RHN with $g_R = g_L$; for $g_R \neq g_L$, the lifetime has to be rescaled by the factor of $(g_R/g_L)^{-4}$.

events to be 10. Note that in Figure C.23 even when the heavy W_R is off-shell, i.e. $m_{W_R} \gtrsim 5$ TeV, the light RHN could yet be produced abundantly. For the purpose of illustration, we also show the proper lifetime of RHN for $g_R = g_L$, estimated from Eq. (C.2); for the values of $g_R \neq g_L$ the lifetime should be rescaled via $(g_R/g_L)^{-4}$ accordingly. Depending on g_R , the general-purpose detectors at LHC could probe the lifetime τ_N^0 from ~ 10 m to below 0.01 cm, after taking into consideration the large Lorentz boost factor E_N/m_N . The RH sector can be probed up to $m_{W_R} \simeq 20$ TeV for a large $g_R/g_L = 1.5$.

We also show the sensitivity contours for MATHUSLA in Figure C.23, assuming at least 4 signal events. Though the effective cross section is smaller (due to its smaller size), MATHUSLA is sensitive to lighter RHN with mass as low as ~ 1 GeV, and could effectively probe a complementary parameter space of LR seesaw with GeV-scale light RHNs.

References

- [1] P. Minkowski, Phys. Lett. B **67**, 421 (1977).
- [2] R. N. Mohapatra and G. Senjanović, Phys. Rev. Lett. **44**, 912 (1980).
- [3] T. Yanagida, Conf. Proc. C **7902131**, 95 (1979).
- [4] M. Gell-Mann, P. Ramond and R. Slansky, Conf. Proc. C **790927**, 315 (1979) [arXiv:1306.4669 [hep-th]].
- [5] S. L. Glashow, NATO Sci. Ser. B **61**, 687 (1980).
- [6] J. C. Pati and A. Salam, Phys. Rev. D **10**, 275 (1974).
- [7] R. N. Mohapatra and J. C. Pati, Phys. Rev. D **11** 2558 (1975).
- [8] G. Senjanović and R. N. Mohapatra, Phys. Rev. D **12** 1502 (1975).
- [9] J. F. Gunion, B. Kayser, R. N. Mohapatra, N. G. Deshpande, J. Grifols, A. Mendez, F. I. Olness and P. B. Pal, PRINT-86-1324 (UC,DAVIS).
- [10] N. G. Deshpande, J. F. Gunion, B. Kayser and F. I. Olness, Phys. Rev. D **44**, 837 (1991).

- [11] P. S. B. Dev, R. N. Mohapatra and Y. Zhang, JHEP **1605**, 174 (2016) [arXiv:1602.05947 [hep-ph]].
- [12] O. Fischer, Mod. Phys. Lett. A **32**, no. 06, 1750035 (2017) [arXiv:1607.00282 [hep-ph]].
- [13] G. Aad *et al.* [ATLAS and CMS Collaborations], JHEP **1608**, 045 (2016) [arXiv:1606.02266 [hep-ex]].
- [14] P. S. B. Dev, R. N. Mohapatra and Y. Zhang, arXiv:1612.09587 [hep-ph].
- [15] D. Chang, R. N. Mohapatra and M. K. Parida, Phys. Rev. Lett. **52**, 1072 (1984).
- [16] A. Maiezza, G. Senjanović and J. C. Vasquez, arXiv:1612.09146 [hep-ph].
- [17] V. Khachatryan *et al.* [CMS Collaboration], Eur. Phys. J. C **74**, 3149 (2014) [arXiv:1407.3683 [hep-ex]].
- [18] G. Aad *et al.* [ATLAS Collaboration], JHEP **1507**, 162 (2015) [arXiv:1506.06020 [hep-ex]].
- [19] V. Khachatryan *et al.* [CMS Collaboration], arXiv:1612.01190 [hep-ex].
- [20] S. Bertolini, A. Maiezza and F. Nesti, Phys. Rev. D **89**, no. 9, 095028 (2014) [arXiv:1403.7112 [hep-ph]].
- [21] I. Z. Rothstein, Nucl. Phys. B **358**, 181 (1991).
- [22] R. Kuchimanchi, Phys. Rev. D **91**, no. 7, 071901 (2015) [arXiv:1408.6382 [hep-ph]].
- [23] J. Chakraborty, J. Gluza, T. Jelinski and T. Srivastava, Phys. Lett. B **759**, 361 (2016) [arXiv:1604.06987 [hep-ph]].
- [24] A. Maiezza, M. Nemeššek and F. Nesti, Phys. Rev. D **94**, no. 3, 035008 (2016) [arXiv:1603.00360 [hep-ph]].
- [25] S. R. Coleman and E. J. Weinberg, Phys. Rev. D **7**, 1888 (1973).
- [26] A. D. Linde, JETP Lett. **23**, 64 (1976).
- [27] S. Weinberg, Phys. Rev. Lett. **36**, 294 (1976).
- [28] M. Holthausen, M. Lindner and M. A. Schmidt, Phys. Rev. D **82**, 055002 (2010) [arXiv:0911.0710 [hep-ph]].
- [29] J. A. Casas and A. Ibarra, Nucl. Phys. B **618**, 171 (2001) [hep-ph/0103065].
- [30] A. Maiezza, M. Nemeššek and F. Nesti, Phys. Rev. Lett. **115**, 081802 (2015) [arXiv:1503.06834 [hep-ph]].
- [31] M. Nemeššek, F. Nesti and J. C. Vasquez, arXiv:1612.06840 [hep-ph].
- [32] P. S. B. Dev, R. N. Mohapatra and Y. Zhang, JHEP **1602**, 186 (2016) [arXiv:1512.08507 [hep-ph]].
- [33] G. Senjanović and V. Tello, Phys. Rev. Lett. **114**, no. 7, 071801 (2015) [arXiv:1408.3835 [hep-ph]].
- [34] G. Senjanović and V. Tello, Phys. Rev. D **94**, no. 9, 095023 (2016) [arXiv:1502.05704 [hep-ph]].
- [35] P. A. R. Ade *et al.* [Planck Collaboration], Astron. Astrophys. **594**, A13 (2016) [arXiv:1502.01589 [astro-ph.CO]].
- [36] L. Heurtier and Y. Zhang, JCAP **1702**, no. 02, 042 (2017) [arXiv:1609.05882 [hep-ph]].
- [37] Y. Zhang, H. An, X. Ji and R. N. Mohapatra, Nucl. Phys. B **802**, 247 (2008) [arXiv:0712.4218 [hep-ph]].
- [38] R. Babich, N. Garron, C. Hoelbling, J. Howard, L. Lellouch and C. Rebbi, Phys. Rev. D **74**, 073009 (2006) [hep-lat/0605016].
- [39] A. J. Buras, S. Jager and J. Urban, Nucl. Phys. B **605**, 600 (2001) [hep-ph/0102316].
- [40] C. Patrignani *et al.* (Particle Data Group), Chin. Phys. C, **40**, 100001 (2016).
- [41] D. Becirevic, V. Gimenez, G. Martinelli, M. Papinutto and J. Reyes, JHEP **0204** (2002) 025 [hep-lat/0110091].
- [42] J. Charles *et al.*, Phys. Rev. D **91**, no. 7, 073007 (2015) [arXiv:1501.05013 [hep-ph]].
- [43] F. Bezrukov and D. Gorbunov, JHEP **1005**, 010 (2010) [arXiv:0912.0390 [hep-ph]].
- [44] J. D. Clarke, R. Foot and R. R. Volkas, JHEP **1402**, 123 (2014) [arXiv:1310.8042 [hep-ph]].
- [45] M. J. Dolan, F. Kahlhoefer, C. McCabe and K. Schmidt-Hoberg, JHEP **1503**, 171 (2015) Erratum: [JHEP **1507**, 103 (2015)] [arXiv:1412.5174 [hep-ph]].
- [46] E. Izaguirre, T. Lin and B. Shuve, arXiv:1611.09355 [hep-ph].
- [47] X. G. He, J. Tandean and G. Valencia, Phys. Rev. D **74**, 115015 (2006) [hep-ph/0610274].
- [48] A. Z. Dubnickova, S. Dubnicka, E. Goudzovski, V. N. Pervushin and M. Secansky, Phys. Part. Nucl. Lett. **5**, 76 (2008) [hep-ph/0611175].
- [49] J. R. Batley *et al.* [NA48/2 Collaboration], Phys. Lett. B **677**, 246 (2009) [arXiv:0903.3130 [hep-ex]].
- [50] J. R. Batley *et al.* [NA48/2 Collaboration], Phys. Lett. B **697**, 107 (2011) [arXiv:1011.4817 [hep-ex]].
- [51] J. M. Gerard, C. Smith and S. Trine, Nucl. Phys. B **730**, 1 (2005) [hep-ph/0508189].
- [52] C. Lazzeroni *et al.* [NA62 Collaboration], Phys. Lett. B **732**, 65 (2014) [arXiv:1402.4334 [hep-ex]].

- [53] V. V. Anisimovsky *et al.* [E949 Collaboration], Phys. Rev. Lett. **93**, 031801 (2004) [hep-ex/0403036].
- [54] A. V. Artamonov *et al.* [E949 Collaboration], Phys. Rev. Lett. **101**, 191802 (2008) [arXiv:0808.2459 [hep-ex]].
- [55] A. V. Artamonov *et al.* [BNL-E949 Collaboration], Phys. Rev. D **79**, 092004 (2009) [arXiv:0903.0030 [hep-ex]].
- [56] A. V. Artamonov *et al.* [E949 Collaboration], Phys. Rev. D **72**, 091102 (2005) [hep-ex/0506028].
- [57] S. Adler *et al.* [E949 and E787 Collaborations], Phys. Rev. D **77**, 052003 (2008) [arXiv:0709.1000 [hep-ex]].
- [58] G. Anelli *et al.*, CERN-SPSC-2005-013, CERN-SPSC-P-326.
- [59] A. J. Buras, D. Buttazzo, J. Girrbach-Noe and R. Knegjens, JHEP **1511**, 033 (2015) [arXiv:1503.02693 [hep-ph]].
- [60] A. Alavi-Harati *et al.* [KTeV Collaboration], Phys. Rev. Lett. **93**, 021805 (2004) [hep-ex/0309072].
- [61] A. Alavi-Harati *et al.* [KTeV Collaboration], Phys. Rev. Lett. **84**, 5279 (2000) [hep-ex/0001006].
- [62] E. Abouzaid *et al.* [KTeV Collaboration], Phys. Rev. D **77**, 112004 (2008) [arXiv:0805.0031 [hep-ex]].
- [63] T. Alexopoulos *et al.* [KTeV Collaboration], Phys. Rev. D **70**, 092006 (2004) [hep-ex/0406002].
- [64] P. Ball and R. Zwicky, Phys. Rev. D **71**, 014015 (2005) [hep-ph/0406232].
- [65] A. Ali, P. Ball, L. T. Handoko and G. Hiller, Phys. Rev. D **61**, 074024 (2000) [hep-ph/9910221].
- [66] B. Aubert *et al.* [BaBar Collaboration], Phys. Rev. Lett. **91**, 221802 (2003) [hep-ex/0308042].
- [67] J.-T. Wei *et al.* [Belle Collaboration], Phys. Rev. Lett. **103**, 171801 (2009) [arXiv:0904.0770 [hep-ex]].
- [68] R. Aaij *et al.* [LHCb Collaboration], JHEP **1302**, 105 (2013) [arXiv:1209.4284 [hep-ex]].
- [69] B. Aubert *et al.* [BaBar Collaboration], Nucl. Instrum. Meth. A **479**, 1 (2002) [hep-ex/0105044].
- [70] T. Abe *et al.* [Belle-II Collaboration], arXiv:1011.0352 [physics.ins-det].
- [71] A. A. Alves, Jr. *et al.* [LHCb Collaboration], JINST **3**, S08005 (2008).
- [72] R. Ammar *et al.* [CLEO Collaboration], Phys. Rev. Lett. **87**, 271801 (2001) [hep-ex/0106038].
- [73] J. P. Lees *et al.* [BaBar Collaboration], Phys. Rev. D **87**, no. 11, 112005 (2013) [arXiv:1303.7465 [hep-ex]].
- [74] W. Altmannshofer, A. J. Buras, D. M. Straub and M. Wick, JHEP **0904**, 022 (2009) [arXiv:0902.0160 [hep-ph]].
- [75] W. Altmannshofer, P. Paradisi and D. M. Straub, JHEP **1204**, 008 (2012) [arXiv:1111.1257 [hep-ph]].
- [76] V. Khachatryan *et al.* [CMS and LHCb Collaborations], Nature **522**, 68 (2015) [arXiv:1411.4413 [hep-ex]].
- [77] R. Aaij *et al.* [LHCb Collaboration], arXiv:1703.05747 [hep-ex].
- [78] J. I. Aranda, A. Flores-Tlalpa, F. Ramirez-Zavaleta, F. J. Tlachino, J. J. Toscano and E. S. Tututi, Phys. Rev. D **79**, 093009 (2009) [arXiv:0905.4767 [hep-ph]].
- [79] J. I. Aranda, J. Montano, F. Ramirez-Zavaleta, J. J. Toscano and E. S. Tututi, Phys. Rev. D **82**, 054002 (2010) [arXiv:1005.5452 [hep-ph]].
- [80] P. del Amo Sanchez *et al.* [BaBar Collaboration], Phys. Rev. D **83**, 032006 (2011) [arXiv:1010.2229 [hep-ex]].
- [81] D. Dutta *et al.* [Belle Collaboration], Phys. Rev. D **91**, no. 1, 011101 (2015) [arXiv:1411.7771 [hep-ex]].
- [82] J. P. Lees *et al.* [BaBar Collaboration], Phys. Rev. D **87**, no. 3, 031102 (2013) Erratum: [Phys. Rev. D **87**, no. 5, 059903 (2013)] [arXiv:1210.0287 [hep-ex]].
- [83] J. P. Lees *et al.* [BaBar Collaboration], Phys. Rev. D **88**, no. 7, 071102 (2013) [arXiv:1210.5669 [hep-ex]].
- [84] J. P. Lees *et al.* [BaBar Collaboration], Phys. Rev. Lett. **107**, 221803 (2011) [arXiv:1108.3549 [hep-ex]].
- [85] F. Wilczek, Phys. Rev. Lett. **39**, 1304 (1977).
- [86] C. Y. Chen, M. Pospelov and Y. M. Zhong, arXiv:1701.07437 [hep-ph].
- [87] F. Bergsma *et al.* [CHARM Collaboration], Phys. Lett. **157B**, 458 (1985).
- [88] S. Alekhin *et al.*, Rept. Prog. Phys. **79**, no. 12, 124201 (2016) [arXiv:1504.04855 [hep-ph]].
- [89] C. Adams *et al.* [LBNE Collaboration], arXiv:1307.7335 [hep-ex].
- [90] D. Gorbunov and M. Shaposhnikov, JHEP **0710**, 015 (2007) Erratum: [JHEP **1311**, 101 (2013)] [arXiv:0705.1729 [hep-ph]].
- [91] A. Falkowski, C. Gross and O. Lebedev, JHEP **1505**, 057 (2015) [arXiv:1502.01361 [hep-ph]].

- [92] S. Profumo, M. J. Ramsey-Musolf, C. L. Wainwright and P. Winslow, *Phys. Rev. D* **91**, no. 3, 035018 (2015) [arXiv:1407.5342 [hep-ph]].
- [93] M. E. Peskin, arXiv:1207.2516 [hep-ph].
- [94] H. Baer *et al.*, arXiv:1306.6352 [hep-ph].
- [95] J. Jaeckel and M. Spannowsky, *Phys. Lett. B* **753**, 482 (2016) [arXiv:1509.00476 [hep-ph]].
- [96] M. Acciarri *et al.* [L3 Collaboration], *Phys. Lett. B* **353**, 136 (1995).
- [97] M. Bicer *et al.* [TLEP Design Study Working Group], *JHEP* **1401**, 164 (2014) [arXiv:1308.6176 [hep-ex]].
- [98] V. Khachatryan *et al.* [CMS Collaboration], *JHEP* **1604**, 035 (2016) [arXiv:1511.03951 [hep-ex]].
- [99] U. Ellwanger and M. Rodriguez-Vazquez, *JHEP* **1602**, 096 (2016) [arXiv:1512.04281 [hep-ph]].
- [100] K. S. Babu and S. Jana, arXiv:1612.09224 [hep-ph].
- [101] P. S. Bhupal Dev and R. N. Mohapatra, *Phys. Rev. Lett.* **115**, no. 18, 181803 (2015) [arXiv:1508.02277 [hep-ph]].
- [102] J. Alwall *et al.*, *JHEP* **1407**, 079 (2014) [arXiv:1405.0301 [hep-ph]].
- [103] G. Aad *et al.* [ATLAS Collaboration], arXiv:0901.0512 [hep-ex].
- [104] G. L. Bayatian *et al.* [CMS Collaboration], *J. Phys. G* **34**, 995 (2007).
- [105] S. Chatrchyan *et al.* [CMS Collaboration], *JINST* **3**, S08004 (2008).
- [106] B. Dasgupta, J. Kopp and P. Schwaller, *Eur. Phys. J. C* **76**, no. 5, 277 (2016) [arXiv:1602.04692 [hep-ph]].
- [107] Y. Tsai, L. T. Wang and Y. Zhao, arXiv:1603.00024 [hep-ph].
- [108] H. Fukuda, M. Ibe, O. Jinnouchi and M. Nojiri, arXiv:1607.01936 [hep-ph].
- [109] J. P. Chou, D. Curtin and H. J. Lubatti, arXiv:1606.06298 [hep-ph].
- [110] A. Coccaro, D. Curtin, H. J. Lubatti, H. Russell and J. Shelton, arXiv:1605.02742 [hep-ph].
- [111] N. Arkani-Hamed, T. Han, M. Mangano and L. T. Wang, *Phys. Rept.* **652**, 1 (2016) [arXiv:1511.06495 [hep-ph]].
- [112] T. Golling *et al.*, arXiv:1606.00947 [hep-ph].
- [113] R. Contino *et al.*, arXiv:1606.09408 [hep-ph].
- [114] B. Batell, M. Pospelov and A. Ritz, *Phys. Rev. D* **83**, 054005 (2011) [arXiv:0911.4938 [hep-ph]].
- [115] The ATLAS collaboration [ATLAS Collaboration], ATLAS-CONF-2016-045.
- [116] CMS Collaboration [CMS Collaboration], CMS-PAS-EXO-16-031.
- [117] S. Patra, F. S. Queiroz and W. Rodejohann, *Phys. Lett. B* **752**, 186 (2016) [arXiv:1506.03456 [hep-ph]].
- [118] M. Lindner, F. S. Queiroz and W. Rodejohann, *Phys. Lett. B* **762**, 190 (2016) [arXiv:1604.07419 [hep-ph]].
- [119] W. Y. Keung and G. Senjanović, *Phys. Rev. Lett.* **50**, 1427 (1983).
- [120] A. Ferrari *et al.*, *Phys. Rev. D* **62**, 013001 (2000).
- [121] M. Nemevsek, F. Nesti, G. Senjanovic and Yue Zhang, *Phys. Rev. D* **83**, 115014 (2011) [arXiv:1103.1627 [hep-ph]].
- [122] S. P. Das, F. F. Deppisch, O. Kittel and J. W. F. Valle, *Phys. Rev. D* **86**, 055006 (2012) [arXiv:1206.0256 [hep-ph]].
- [123] J. A. Aguilar-Saavedra and F. R. Joaquim, *Phys. Rev. D* **86**, 073005 (2012) [arXiv:1207.4193 [hep-ph]].
- [124] C. Y. Chen, P. S. B. Dev and R. N. Mohapatra, *Phys. Rev. D* **88**, 033014 (2013) [arXiv:1306.2342 [hep-ph]].
- [125] F. F. Deppisch, P. S. B. Dev and A. Pilaftsis, *New J. Phys.* **17**, 075019 (2015) [arXiv:1502.06541 [hep-ph]].
- [126] J. Gluza and T. Jeliński, *Phys. Lett. B* **748**, 125 (2015) [arXiv:1504.05568 [hep-ph]].
- [127] J. N. Ng, A. de la Puente and B. W. P. Pan, *JHEP* **1512**, 172 (2015) [arXiv:1505.01934 [hep-ph]].
- [128] P. S. B. Dev, D. Kim and R. N. Mohapatra, *JHEP* **1601**, 118 (2016) [arXiv:1510.04328 [hep-ph]].
- [129] J. Gluza, T. Jelinski and R. Szafron, *Phys. Rev. D* **93**, no. 11, 113017 (2016) [arXiv:1604.01388 [hep-ph]].
- [130] M. Lindner, F. S. Queiroz, W. Rodejohann and C. E. Yaguna, *JHEP* **1606**, 140 (2016) [arXiv:1604.08596 [hep-ph]].

- [131] M. Mitra, R. Ruiz, D. J. Scott and M. Spannowsky, Phys. Rev. D **94**, 095016 (2016) [arXiv:1607.03504 [hep-ph]].
- [132] S. S. Biswal and P. S. B. Dev, arXiv:1701.08751 [hep-ph].
- [133] G. Azuelos, K. Benslama and J. Ferland, J. Phys. G **32**, no. 2, 73 (2006) [hep-ph/0503096].
- [134] D. W. Jung and K. Y. Lee, Phys. Rev. D **78**, 015022 (2008) [arXiv:0802.1572 [hep-ph]].
- [135] P. Fileviez Perez, T. Han, G. y. Huang, T. Li and K. Wang, Phys. Rev. D **78**, 015018 (2008) [arXiv:0805.3536 [hep-ph]].
- [136] G. Bambhaniya, J. Chakraborty, J. Gluza, M. Kordiaczyska and R. Szafron, JHEP **1405**, 033 (2014) [arXiv:1311.4144 [hep-ph]].
- [137] B. Dutta, R. Eusebi, Y. Gao, T. Ghosh and T. Kamon, Phys. Rev. D **90**, 055015 (2014) [arXiv:1404.0685 [hep-ph]].
- [138] G. Bambhaniya, J. Chakraborty, J. Gluza, T. Jelinski and M. Kordiaczynska, Phys. Rev. D **90**, no. 9, 095003 (2014) [arXiv:1408.0774 [hep-ph]].
- [139] G. Bambhaniya, J. Chakraborty, J. Gluza, T. Jelinski and R. Szafron, Phys. Rev. D **92**, no. 1, 015016 (2015) [arXiv:1504.03999 [hep-ph]].
- [140] CMS Collaboration [CMS Collaboration], CMS-PAS-HIG-16-036.
- [141] O. Castillo-Felisola, C. O. Dib, J. C. Helo, S. G. Kovalenko and S. E. Ortiz, Phys. Rev. D **92**, no. 1, 013001 (2015) [arXiv:1504.02489 [hep-ph]].
- [142] J. C. Helo, M. Hirsch and S. Kovalenko, Phys. Rev. D **89**, 073005 (2014) Erratum: [Phys. Rev. D **93**, no. 9, 099902 (2016)] [arXiv:1312.2900 [hep-ph]].
- [143] S. Antusch, E. Cazzato and O. Fischer, arXiv:1612.02728 [hep-ph].